Fundamental studies for Autologous Tumor Vaccine therapy

自家がんワクチン療法に対する基礎的研究

The United Graduate School of Veterinary Science

Yamaguchi University

Tsutomu TANAKA

September 2015

Doctor's Thesis

The United Graduate School of Veterinary Science

Yamaguchi University

Fundamental studies for Autologous Tumor Vaccine therapy

自家がんワクチン療法に対する基礎的研究

Tsutomu Tanaka

September 2015

Laboratory of Veterinary Neurology and Oncology,

Department of Veterinary Clinical Medicine,

Tottori University

Contents

Page No.

Publications 1

Abstract 2

General introduction 4

Reference 5

Chapter 1

Hsp90 targets a chaperoned peptide to the static early endosome for efficient cross-presentation by human dendritic cells.

Abstract · **6**

1. Introduction · **7**

2. Materials and methods · **9**

3. Results · **18**

4. Discussion · **24**

References · **28**

Figures legend · **30**

Figure and table · **35**

Chapter 2

Cancer-associated oxidoreductase ERO1-α drives the production of tumor-promoting myeloid-derived suppressor cells via oxidative protein folding.

Abstract · 42

1. Introduction · 43

2. Materials and methods · 46

3. Results · 54

4. Discussion · 63

References · 68

Figures legend • 71

Figures • 78

Supplemental materials methods • 88

Supplemental Figures legend and Table legend • • • • • • • • • • • • • • 90

Supplemental Figure and Table • 93

Conclusions • 97

Acknowledgements • 98

Publications

The contents of this thesis were published in the following journals.

Chapter I

Tsutomu Tanaka, Koichi Okuya, Goro Kutomi, Akari Takaya, Toshimitsu Kajiwara, Takayuki Kanaseki, Tomohide Tsukahara, Yoshihiko Hirohashi, Toshihiko Torigoe, Koichi Hirata, Yoshiharu Okamoto, Noriyuki Sato, and Yasuaki Tamura: Hsp90 targets a chaperoned peptide to the static early endosome for efficient cross-presentation by human dendritic cells. Cancer Science, 106, pp 18-24, 2015

Chapter II

Tsutomu Tanaka, Toshimitsu Kajiwara, Toshihiko Torigoe, Yoshiharu Okamoto, Noriyuki Sato and Yasuaki Tamura: Cancer-associated oxidoreductase ERO1-a drives the production of tumor-promoting myeloid-derived suppressor cells via oxidative protein folding. The Journal of Immunology, 194, pp 2004-2010, 2015

Abstract

Recently, life-span of animals is prolonged by the progress of veterinary science, the improvement of feeding environment and the diffusion of vaccine. Therefore, various diseases such as tumors, which occur in aging animals, were increased. Standard treatments against tumors are surgery, radiotherapy treatment and chemotherapy in veterinary field same as in medical field. However, most of clinician in medical field and veterinary field recognize that it is impossible to treat all tumors by using only these three major treatments. Various therapies are studied as well as standard treatments in medical field. Immune therapy is the one of these new therapies. Immune therapy is the therapy without serious side effects and is studied and used in clinical field of medicine. In late years, interest for immune therapy is increased in veterinary field.

Autologous Tumor Vaccines (ATVs) treatment is the one of immune therapy. In ATVs treatment, patients are immunized by using antigen which is extracted from own tumor tissue to prevent repullulation. As we can use formalin fixed tumor tissue as the tissue extracted antigen from, acquisition of tumor tissue is easy. In our laboratory, we analyzed therapy effect of ATVs treatment by using about 800 cases of spontaneity

tumor of canine and feline. In the study using clinical cases, I observed that minority of these cases did not have any effect against treatment using ATVs treatment. We supposed that these minority cases occurred for deficiency of amount of vaccination antigen and immunosuppression of animals.

In chapter I, I found that an Hsp90-cancer antigen peptide complex was efficiently cross-presented by human monocyte-derived DCs and induced peptide-specific CTLs. Furthermore, we observed that the internalized Hsp90-peptide complex was strictly sorted to the Rab5^{+}, EEA1^{+} static early endosome and the Hsp90-chaperoned peptide was processed and bound to MHC class I molecules through a endosome-recycling pathway. Our data indicate that targeting of the antigen to a “static” early endosome by Hsp90 is essential for efficient cross-presentation.

In chapter II, I found that endoplasmic reticulum (ER) disulfide oxidase ERO1-α was overexpressed in a variety of tumor types. My results suggest that overexpression of ERO1-α in the tumor inhibits T cell response by recruiting PMN-MDSCs via regulation of MDSC-prone cytokines and chemokines by regulating at the post-transcriptional level.

From these studies, it is considered that ATVs treatment becomes more effective.

General introduction

Recently, life-span of animals is prolonged by the progress of veterinary science, the improvement of feeding environment and the diffusion of vaccine. Therefore, various diseases such as tumors, which occur in aging animals, were increased. Standard treatments against tumors are surgery, radiotherapy treatment and chemotherapy in veterinary field same as in medical field. However, most of clinician in medical field and veterinary field recognize that it is impossible to treat all tumors by using only these three major treatments. Various therapies such as photodynamic hyperthermia, hyperthermia treatment, diet therapy are studied as well as standard treatments in medical field. Immune therapy is the one of these new therapies. Immune therapy is the therapy without serious side effects and is studied and used in clinical field of medicine. In late years, interest for immune therapy is increased in veterinary field.

Autologous Tumor Vaccines (ATVs) is the one of immune therapy. In ATVs, patients are immunized by using antigen which is extracted from own tumor tissue to prevent repullulation (Kim et al., 1998). As we can use formalin fixed tumor tissue as the tissue extracted antigen from, acquisition of tumor tissue is easy. In medical field,

simpleness of acquisition affects attention as the new therapy for tumor. In our laboratory, we analyzed therapy effect of ATVs by using about 800 cases of spontaneity tumor of canine and feline. Majority of these cases were prolonged in overall survival and disease free survival. However, we observed that minority of these cases did not have any effect against treatment using ATVs. We supposed that these minority cases occurred for deficiency of amount of vaccination antigen and immunosuppression of animals. Accordingly, we hypothesize that these minority cases have good effects when antigenic presentation are more efficient and immunosuppression is removed.

In this study, I performed fundamental researches to make treatment using ATVs into more effective treatment. I present that Hsp90 influence antigen presentation in chapter I, and that Endoplasmic reticulum (ER) disulfide oxidase ERO1-α influence immunosuppression by polymorphonuclear myeloid-derived suppressor cells in chapter II.

Reference

Kim C, Matsumura M, Saijo K, Ohno T: In vitro induction of HLA-A2402-restricted and carcinoembryonic-antigen-specific cytotoxic T lymphocytes on fixed autologous peripheral blood cells. Cancer Immunol Immunother 47:90-96, 1998.

Chapter I

Hsp90 targets a chaperoned peptide to the static early endosome for efficient cross-presentation by human dendritic cells.

Abstract

The presentation of an exogenous antigen in a major histocompatibility complex class-I- restricted fashion to $CD8^+$ T cells is called cross-presentation. Heat shock proteins (HSPs) such as Hsp70, gp96 and Hsp90 have been shown to elicit efficient cytotoxic T lymphocyte (CTL) responses by cross-presentation via an as yet entirely unknown mechanism. Hsp90 is the most abundant cytosolic HSP and is known to act as a molecular chaperone. We have demonstrated that a tumor antigen peptide complexed with Hsp90 could be cross-presented by dendritic cells (DCs) via an endosomal pathway in a murine system. However, it has not been determined whether human DCs also cross-present an Hsp90-peptide complex and induce peptide-specific CTLs. In this

study, we found that an Hsp90-cancer antigen peptide complex was efficiently cross-presented by human monocyte-derived DCs and induced peptide-specific CTLs. Furthermore, we observed that the internalized Hsp90-peptide complex was strictly sorted to the Rab5$^+$, EEA1$^+$ static early endosome and the Hsp90-chaperoned peptide was processed and bound to MHC class I molecules through a endosome-recycling pathway. Our data indicate that targeting of the antigen to a "static" early endosome by Hsp90 is essential for efficient cross-presentation.

1. Introduction

The generation of specific CD8$^+$ CTLs is thought to play a key role in the control of virus-infected cells and tumors. However, immunization with peptides or recombinant proteins generally fails to elicit CTLs because an immunized antigen acts as an exogenous antigen. Generally, an exogenous antigen enters the MHC class II pathway and is presented to CD4$^+$ T cells in the context of MHC class II molecules. However, professional antigen-presenting cells (APCs), particularly dendritic cells (DCs), can take up exogenous antigens and present them on their MHC class I

molecules. This process is called cross-presentation and plays an important role in the control of virus-infected cells and tumor growth[1]. There are two pathways of cross-presentation: cytosolic (ER-Golgi-dependent) and vacuolar (endosomal) pathways[2, 3]. One of the reasons for inefficiency of a vaccine strategy is that the vaccine antigen is usually administered as an exogenous antigen, and it is therefore difficult to introduce the vaccine antigen into the cross-presentation pathway. To overcome this problem, various methods have been developed to target an exogenous Ag into the endogenous MHC class I-restricted pathway. In our previous studies, we demonstrated that extracellular Hsp90-peptide complexes are efficiently cross-presented via the endosome-recycling pathway[4]. In this Hsp90-mediated cross-presentation, the receptor-dependent endocytosed Hsp90-peptide complex was transferred to the early endosome in which a cysteine protease such as cathepsin S processed the precursor peptide. The resulting MHC class I epitope was transferred onto recycling MHC class I molecules, thereby resulting in the expression of an MHC class I-epitope complex on the cell surface. Furthermore, we have shown that immunization with Hsp90-tumor antigen peptide complexes induces Ag-specific CTL responses and strong antitumor

immunity *in vivo*. However, how the Hsp90-peptide complex is sorted out after receptor-dependent endocytosis remains unclear. In the present work, we found that Hsp90 complexed with a human tumor antigen peptide derived from survivin-2B[5, 6] is cross-presented by human monocyte-derived DCs, (Mo-DCs) resulting in the stimulation of peptide-specific CTLs. In addition, we found that Hsp90 targets a chaperoned antigen peptide into the "static" early endosome within Mo-DCs, resulting in cross-presentation of the antigenic peptide through the recycling pathway.

2. **Materials and Methods**

The study protocol was approved by the Clinic Institutional Ethical Review Board of the Medical Institute of Bioregulation, Sapporo Medical University (Sapporo, Japan). The patients and their families as well as healthy donors gave informed consent for the use of blood samples in our research.

2.1 Patient treatment

The patients were vaccinated with survivin-$2B_{80-88}$ (1 mg) plus Montanide ISA 51

(1 ml) subcutaneously four times at 14-day intervals. In addition, IFN-α (3,000,000 IU) was administered subcutaneously twice a week close to the site of vaccination. Montanide ISA 51 was purchased from Seppic (Paris, France) and IFN-α was purchased from Dainippon-Sumitomo Pharmaceutical Co. (Osaka, Japan). Hematological examinations were conducted before and after each vaccination.

2.2 Induction of human monocyte-derived immature dendritic cells.

Autologous monocytes were purified from peripheral blood mononuclear cells (PBMCs) from each patient that were isolated using Lymphoprep (Nycomed, Oslo, Norway). Monocytes (1 x 10^4/well) in a 24-well plate were cultured in complete RPMI-1640 with 10% FCS and GM-CSF (1,000 units/mL) and IL-4 (1,000 units/mL) for 7 days. The medium with GM-CSF and IL-4 was gently replaced on day 2 and day 4. Human recombinant GM-CSF was a kind gift from Kirin (Tokyo, Japan). Human recombinant IL-4 was purchased from Invitrogen (Carlsbad, CA).

2.3 Peptides and proteins.

The following peptides were used (underlined sequences representing the precise MHC class I-binding epitope): survivin-2B$_{80-88}$ (AYACNTSTL), survivin-2B$_{75-93}$ (GPGTVAYACNTSTLGGRGG). All peptides were purchased from SIGMA genosys (Ishikari, Japan). Human Hsp90 was purchased from StressGen (Ann Arbor, MI). Human low-density lipoprotein (LDL) was purchased from SIGMA-Aldrich (St. Louis, MO) and stored at 20 mg/ml in PBS at -80°C.

2.4 Antibodies.

Confocal laser microscopy was used to detect organelles with specific antibodies: an anti-Rab5 pAb (MBL, Nagoya. Japan) and EEA1 (Abcam, Cambridge, MA) for early endosomes and anti-LAMP-1 pAb (Santa Cruz Biotechnology, Santa Cruz, CA) for late endosomes/lysosomes. Alexa Fluor 594 (Molecular Probes, Eugene, OR) was used for labeling Hsp90 and LDL.

2.5 Generation of Hsp90-peptide complex in vitro.

As previously described[4], Hsp90 was mixed with survivin-2B$_{75-93}$

(GPGTVAYACNTSTLGGRGG) in a 50:1 peptide to protein molar ratio in 0.7 M NaCl containing sodium-phosphate buffer and heated at 45°C for 30 min and then incubated for 30 min at room temperature.

2.6 Establishment of survivin-2B$_{80-88}$-specific CTL clone.

We generated survivin-2B$_{80-88}$-specific CTL clones from a patient with colon cancer (patient 1 in Table 1). PBMCs after the fourth vaccination were isolated from blood samples by Ficoll-Conray density gradient centrifugation. PHA blasts were derived from PBMCs by culturing in AIM-V medium (Invitrogen Corp., Carlsbad, CA) containing 10% human serum, IL-2 (100 units/mL) (Takeda Pharmaceutical Co. Osaka, Japan) and PHA (1 mg/mL, Wako Chemicals, Osaka, Japan) for 3 days, followed by washing and cultivation in the presence of IL-2 (100 units/ml) for 4 days. HLA-A*2402-survivin-2B$_{80-88}$ peptide tetramer (MBL)-positive CTLs were sorted and subsequently cloned to single cells using FACSAria (Becton Dickinson, San Jose, CA). Survivin-2B$_{80-88}$-specific CTL clones were restimulated with survivin-2B$_{80-88}$ peptide-pulsed PHA blasts every 7 days in AIM-V supplemented with 50 U/ml of IL-2.

2.7 In vitro cross-presentation assay.

Human Mo-DCs (1 x 10^5) were pulsed with Hsp90 (400 μg/ml), survivin-$2B_{75-93}$ (400 μg/ml) alone, a complex of Hsp90 (100 μg/ml or 400 μg/ml) and survivin-$2B_{75-93}$ (100 μg/ml or 400 μg/ml), a simple mixture of both or survivin-$2B_{80-88}$ (400 μg/ml) for 2 h at 37°C in 100 μl of Opti-MEM and then fixed for 1 min with 0.01% glutaraldehyde. Fixation was stopped by addition of 2 M L-lysine and the cells were washed 2 times with RPMI-1640 medium and cultured overnight with 1x10^5 survivin-2B peptide-specific CTL clone. Activation of CTLs was measured as IFN-γ production using ELISA. In a dose titration assay, Mo-DCs (1 x 10^5) were loaded with various doses of survivin-$2B_{80-88}$ peptide or Hsp90-precursor peptide (survivin-$2B_{75-93}$) complex for 2 h in 100 μl of Opti-MEM and fixed with 0.01% glutaraldehyde. The cells were washed and cultured overnight with 1 x 10^5 survivin-$2B_{80-88}$-peptide-specific CTL clone. IFN-γ in the culture supernatant was measured using ELISA.

2.8 In vitro stimulation of PBMCs with Mo-DC loaded with Hsp90-precursor peptide

complex.

PBMCs were isolated from eight patients suffering from various types of cancer who had been vaccinated with survivin-2B peptide in our clinical study[7, 8]. These patient's PBMCs were shown to contain survivin-2B-specific $CD8^+$ T cells. PBMCs were stimulated with Mo-DCs loaded with survivin-$2B_{80-88}$ (400 μg/ml), Hsp90 (400 μg/ml), survivin-$2B_{75-93}$ (400 μg/ml), and Hsp90 (100 μg/ml or 400 μg/ml)-survivin-$2B_{75-93}$ (100 μg/ml or 400 μg/ml) complex in AIM V medium (Life Technologies Corp, Grand Island, NY, USA) containing 10% human serum. IL-2 was added at a final concentration of 50 U/mL on days 2, 4, and 6. On day 7 of culture, the PBMCs were analyzed by tetramer staining and ELISPOT assay.

2.9 Assessment of stimulation of antigen-specific CTLs using tetramer assay.

FITC-labeled HLA-A*2402-human immunodeficiency virus (HIV) peptide (RYLRDQQLL) and PE-labeled HLA-A*2402-survivin-$2B_{80-88}$ peptide tetramers were purchased from MBL. For flow cytometric analysis, PBMCs, which were stimulated *in vitro* as described above, were stained with HIV tetramer or survivin-2B tetramer at

37°C for 20 min. Then a PE-Cy5-conjugated anti-CD8 antibody (eBioscience, San Diego, CA) was added at 4°C for 30 min. Cells were washed twice with PBS. After washing, cells were fixed with 0.5% paraformaldehyde and analyzed by flowcytometry using FACScalibur and CellQuest software (Becton Dickinson, San Jose, CA). $CD8^+$ living cells were gated and cells labeled with survivin-2B tetramer were referred to as tetramer-positive cells. The frequency of CTL precursors was calculated as the number of tetramer-positive cells divided by the number of $CD8^+$ T cells.

2.10 Assessment of stimulation of antigen-specific CTLs using ELISPOT assay.

ELISPOT plates were coated sterilely overnight with anti-IFN-γ capture antibody (BD Biosciences, San Jose, CA) at 4°C. The plates were then washed once and blocked with AIM-V medium containing 10% human serum for 2 h at room temperature. CD8-positive T cells separated from patients' PBMCs (5×10^3 cell/well), which were stimulated *in vitro* as described above, were then added to each well along with HLA-A24-transfected T2 (T2-A24) cells (5×10^4 cells/well) that had been preincubated with survivin-$2B_{80-88}$ (10 μg/ml) or HIV with an HIV peptide as a negative control.

After incubation in a 5% CO_2 humidified chamber at 37°C for 24 h, the wells were washed vigorously five times with PBS and incubated with a biotinylated anti-human IFN-γ antibody (R&D systems, Minneapolis, MN) and horseradish peroxidase-conjugated avidin. Spots were visualized and analyzed using KS ELISPOT (Carl Zeiss, Jena, Germany).

2.11 Immunocytological localization of Hsp90-survivin-$2B_{75-93}$ peptide complex.

Hsp90 and LDL were conjugated with Alexa Fluor 594 (Molecular Probes) according to the manufacturer's instructions. Mo-DCs were incubated at 37°C with Alexa Fluor 594 labeled-Hsp90 (20 μg) complexed with survivin-$2B_{75-93}$ peptide (20 μg) for 1 h. Following incubation, cells were washed twice with ice-cold PBS and fixed with ice-cold acetone for 1 min. Organelles were stained with an anti-Rab5 pAb and EEA1 mAb for early endosomes and anti-LAMP-1 pAb for late endosomes followed by Alexa 488-conjugated goat anti-rabbit IgG (Molecular Probes) or anti-mouse IgG (Molecular Probes) and then visualized with a Bio-Rad MRC1024ES confocal scanning laser microscope system (Bio-Rad, Richmond, CA). For evaluation of colocalization, a

single z-plane of one cell was evaluated. For each protein and organelle combination, a total of 150 cells (50 cells from three independent experiments) were analyzed.

2.12 Inhibition studies

Mo-DCs were pre-incubated with chloroquine (SIGMA-Aldrich) or primaquine (ICN Biomedicals, Irvine, CA) at 37°C for 2 h, and then loaded with survivin-$2B_{80-88}$ peptide alone or Hsp90-precursosr peptide (survivin-$2B_{75-83}$) complex for 2 h. The Mo-DCs then fixed, washed and cultured overnight with survivin-$2B_{80-88}$-specific CTL clone. Activation of CTLs was measured as IFN-γ production using ELISA.

2.13 Statistical analysis

All experiments were independently performed three times in triplicate. Results are shown as means +SEM. Comparisons between two groups were performed using Student's *t* test, with a *p* value less than 0.05 considered to be statistically significant.

3. Results

3.1 Hsp90-survivin-2B$_{75-93}$ peptide complex is cross-presented by Mo-DCs in vitro.

We first examined whether human Hsp90 facilitated cross-presentation of the chaperoned precursor peptide by human Mo-DCs. Mo-DCs were pulsed with Hsp90 alone, the survivin-2B$_{75-93}$ precursor peptide alone, a simple mixture of both, a complex of them generated *in vitro* at double concentration, or survivin-2B$_{80-88}$ peptide (for positive control) for 2 h at 37°C and then fixed, washed, and cultured with survivin-2B$_{80-88}$-specific CTL clone. The Hsp90-survivin-2B$_{75-93}$ precursor peptide complex elicited a significant amount of IFN-γ production both at 100 μg/ml and 100 μg/ml, while Hsp90 alone, survivin-2B$_{75-93}$ precursor peptide alone or simple mixture of both did not induce IFN-γ production by CTLs (Fig. 1A). Strikingly, IFN-γ production induced by Hsp90-survivin-2B precursor peptide complex was much greater than that induced by survivin-2B peptide. These results indicated that cross-presentation of survivin-2B-derived peptide was enhanced when an exogenous precursor peptide was complexed to Hsp90. To confirm these observations, we compared the efficacy of CTL activation between survivin-2B$_{80-88}$ peptide and Hsp90-survivin-2B$_{75-93}$ precursor

peptide complex in a dose titration assay (Fig. 1B). We observed that stimulation of the survivin-2B$_{80-88}$-specific CTL clone with Hsp90-survivin-2B$_{75-93}$ precursor peptide complex was more effective than stimulation with survivin-2B$_{80-88}$ peptide at any dose.

3.2 Peptide-specific precursor CTLs are activated by cross-presentation of Hsp90-peptide complex.

Since we demonstrated that Hsp90-survivin-2B$_{75-93}$ precursor peptide complex was efficiently cross-presented, we next examined whether cross-presentation of Hsp90-peptide complex could activate and expand peptide-specific memory CD8^{+} T cells from patients who had been vaccinated with survivin-2B peptide with IFA. Activated and expanded survivin-2B-specific CD8^{+} T cells were detected by tetramer staining. As shown in Fig. 2, the survivin-2B$_{75-93}$ precursor peptide chaperoned by Hsp90 was able to activate and expand survivin-2B-specific memory CD8^{+} T cells more vigorously than was the precursor peptide alone. Interestingly, peptide-specific T-cell frequency was higher when stimulated with Hsp90-survivin-2B$_{75-93}$ precursor peptide complex than that with survivin-2B$_{80-88}$ peptide, indicating that a long peptide

chaperoned by Hsp90 was efficiently cross-presented and was able to stimulate peptide-specific $CD8^+$ T cells. To confirm these observations, we compared the efficacy of activation of survivin-2B-specific memory $CD8^+$ T cells by stimulation with survivin-$2B_{80-88}$, survivin-$2B_{75-93}$ precursor peptide, or Hsp90-survivin-$2B_{75-93}$ precursor peptide complex in eight patients. As shown in Table 1, stimulation with Hsp90-survivin-$2B_{75-93}$ complex could expand survivin-2B-specific memory $CD8^+$ T cells from seven out of eight patients compared with stimulation with survivin-$2B_{75-93}$. More importantly, in six out of eight patients, stimulation with Hsp90-survivin-$2B_{75-93}$ complex expanded survivin-2B-specific memory $CD8^+$ T cells more efficiently compared with stimulation with survivin-$2B_{80-88}$.

3.3 Memory $CD8^+$ T cells activated by cross-presentation of Hsp90-peptide complex become functional peptide-specific CTLs.

To further confirm whether survivin-2B-specific $CD8^+$ T cells activated by Hsp90-mediated cross-presentation were functional or not, we carried out an ELSPOT assay using $CD8^+$ T cells from patient who had been vaccinated with survivin-2B

peptide with IFA. Figure 3 shows that stimulation of $CD8^+$ T cells from patient with Hsp90-survivin-$2B_{75-93}$- precursor peptide complex clearly increased functionally-positive survivin-2B-specific $CD8^+$ T cells compared with stimulation with survivin-$2B_{75-93}$ precursor peptide or survivin-$2B_{80-88}$ peptide. When $CD8^+$ T cells from the patient were stimulated with Hsp90 (400 μg/ml)-precursor peptide (400 μg/ml) complex, the number of IFN-γ-positive spots was less that of $CD8^+$ T cells stimulated with Hsp90 (100 μg/ml)-precursor peptide (100 μg/ml) complex. These results were due to the formation of fused large spots that was observed when stimulated with Hsp90 (400 μg/ml)-precursor peptide (400 μg/ml) complex and therefore the number of ELISPOT counted became smaller than that of Hsp90 (100 μg/ml)-precursor peptide (100 μg/ml) complex. These findings indicated that Hsp90-peptide complex is efficiently cross-presented by human Mo-DCs and is capable of stimulating peptide-specific CTLs.

3.4 Immunocytological localization of Hsp90- survivin$2B_{75-93}$ peptide complex.

For further support of the above-described results, we investigated the intracellular

routing of Hsp90 after uptake of it in DCs, using confocal laser microscopy. Mo-DCs were incubated with Alexa 594-labeled Hsp90- survivin2B$_{75-93}$ peptide complex for 1 hr. Following incubation, the cells were fixed and stained with antibodies against markers for organelle structures including EEA1, Rab5, and LAMP-1. Alexa 594-labeled Hsp90-peptide complex was detected in EEA1^{+}, Rab5^{+}-early endosomes but not in lysosomes (Fig. 4A). Quantitative analysis of the colocalization between the exogenous Hsp90-peptide complex and Rab5, EEA1, and LAMP1 revealed average colocalization incidences of 78.0%, 88.7% and 7.3%, respectively, providing further evidence that the exogenous Hsp90-peptide complex was delivered to the endosome-recycling pathway (Fig. 4B). We also examined the dynamics of Alexa 594-labeled LDL as a positive control protein for the dynamic early endosomal pathway (Fig. 5A and 5B). Alexa594-labeled soluble LDL localized to the Rab5^{+}-early endosome as well as the LAMP-1^{+}-late endosome/lysosome, but not to the EEA1^{+}-compartment, thus indicating the dynamic endosomal pathway. These results indicated that the Hsp90-peptide complex was sorted into the static endosomal pathway, not the dynamic endosomal pathway, within human Mo-DCs. In contrast, the soluble LDL protein, which underwent

degradation, was translocated to the dynamic endosomal pathway. These results suggested that targeting to the "static" early endosome was required for efficient cross-presentation by Mo-DCs.

3.5 Hsp90-peptide complex is cross-presented by human DCs via an endosome-recycling pathway.

We then examined whether Hsp90-precursor peptide complex was cross-presented by human Mo-DCs via an endosomal pathway after targeting to the static early endosome. We used chloroquine for inhibition of endosomal acidification and primaquine for inhibition of the membrane recycling pathway. As shown in Fig. 6A, Mo-DCs that were pre-incubated with increasing concentrations of chloroquine completely blocked cross-presentation of Hsp90-survivin-2B$_{75-93}$ precursor peptide complex but had no substantial effect on survivin-2B$_{80-88}$ peptide presentation. These results indicated that cross-presentation of Hsp90-precursor peptide complex depended on endosomal acidification, possibly including proteolysis by endosomal proteases. Moreover, Mo-DC incubated with primaquine could not present the Hsp90-chaperoned

precursor peptide-derived survivin-2B$_{80-88}$ peptide to CTL (Fig. 6B). These results indicated that the Hsp90-chaperoned precursor peptide or processed peptide entered recycling endosomes and were transferred onto recycling MHC class I molecules.

4. Discussion

It has been demonstrated that immunization with tumor-derived HSPs or HSPs complexed with an antigen peptide/protein elicits tumor- or antigen-specific CD8^{+} T cell responses[1, 9]. Importantly, it has been shown that Hsp70- and gp96-antigen complexes facilitate antigen presentation in association with MHC class I molecule[10-13]. Recently, we[3, 4] and Calderwood's group[14] have demonstrated that Hsp90 also acted as an excellent navigator for associated antigens to enter the cross-presentation pathway in murine system. We here showed that human Hsp90-cancer antigen peptide complex was efficiently cross-presented by human Mo-DCs. These results hold promise for the development of a safe and efficient immunomodulator for cancer immunotherapy. More importantly, we showed that translocation of Hsp90-Ag complex into the static early endosome after endocytosis was crucial for efficient cross-presentation. It has been

shown that the pathway for cross-presentation is comprised of two distinct intracellular routes, a proteasome-TAP-dependent pathway and an endosome-recycling pathway[2, 3]. Recent studies have revealed the pathway in which peptide exchange onto recycling MHC class I molecules occurs within early endosomal compartments[15]. We have shown that Hsp90-peptide complex-mediated[4] and ORP150-peptide complex-mediated[16] cross-presentation was independent of TAP and was sensitive to primaquine, indicating that sorting of peptides onto MHC class I occurs via an endosome-recycling pathway. Very recently, Lakadamyali et al.[17] have shown that early endosomes are comprised of two distinct populations: a dynamic population that is highly mobile on microtubules and matures rapidly toward the late endosome and a static population that matures much more slowly. Cargos destined for degradation, including LDL, EGF, and influenza virus, are internalized and targeted to the Rab5^{+}, EEA1^{-}-dynamic population of early endosomes as we have observed using LDL, thereafter trafficking to Rab7^{+}-late endosmes. In contrast, the recycling ligand transferrin is delivered to Rab5^{+}, EEA1^{+}-static early endosomes, followed by translocation to Rab11^{+}-recycling endosomes. Furthermore, Burgdorf et al. clearly demonstrated that a mannose receptor

introduced OVA specifically into an EEA-1^{+}, Rab5^{+}-stable early endosomal compartment for subsequent cross-presentation[18]. In contrast, pinocytosis conveyed OVA to lysosomes for class II presentation. Of interest, OVA endocytosed by a scavenger receptor did not colocalize with EEA1 but colocalized with LAMP-1 in lysosomes, leading to presentation in the context of MHC class II molecules. We showed that the human Hsp90-peptide complex is targeted into Rab5^{+}, EEA1^{+}-early endosomes after internalization by Mo-DCs, suggesting that preferential sorting to the "static" endosome is necessary for cross-presentation of Hsp90-peptide complexes. In contrast, soluble LDL protein was targeted to the EEA1^{-} and LAMP-1^{+}-dynamic early endosome-late endosome/lysosome pathway, leading to degradation and presentation in the context of MHC class II molecules. These findings suggested that Hsp90 shuttled the chaperoned precursor peptide into the static endosome-recycling pathway, preventing further degradation, followed by transfer of the peptide onto recycling MHC class I molecules. Together, our findings indicate that the role of Hsp90 in cross-presentation is to navigate the associated antigen into static early endosomes within human Mo-DCs. Thus, Hsp90 appears to be a promising natural

immunoactivator for use of cancer vaccine development due to its excellent ability to target human DCs and to induce specific CTLs.

References

[1] Srivastava P. Interaction of heat shock proteins with peptides and antigen presenting cells: chaperoning of the innate and adaptive immune responses. Annu Rev Immunol. 2002; 20: 395-425.

[2] Shen L, Sigal LJ, Boes M, Rock KL. Important role of cathepsin S in generating peptides for TAP-independent MHC class I crosspresentation in vivo. Immunity. 2004; 21: 155-65.

[3] Oura J, Tamura Y, Kamiguchi K, et al. Extracellular heat shock protein 90 plays a role in translocating chaperoned antigen from endosome to proteasome for generating antigenic peptide to be cross-presented by dendritic cells. Int Immunol. 2011; 23: 223-37.

[4] Kurotaki T, Tamura Y, Ueda G, et al. Efficient Cross-Presentation by Heat Shock Protein 90-Peptide Complex-Loaded Dendritic Cells via an Endosomal Pathway. J Immunol. 2007; 179: 1803-13.

[5] Hirohashi Y, Torigoe T, Maeda A, et al. An HLA-A24-restricted cytotoxic T lymphocyte epitope of a tumor-associated protein, survivin. Clin Cancer Res. 2002; 8: 1731-9.

[6] Kameshima H, Tsuruma T, Kutomi G, et al. Immunotherapeutic benefit of alpha-interferon (IFNalpha) in survivin2B-derived peptide vaccination for advanced pancreatic cancer patients. Cancer Sci. 2013; 104: 124-9.

[7] Tsuruma T, Iwayama Y, Ohmura T, et al. Clinical and immunological evaluation of anti-apoptosis protein, survivin-derived peptide vaccine in phase I clinical study for patients with advanced or recurrent breast cancer. J Transl Med. 2008; 6: 24.

[8] Kameshima H, Tsuruma T, Torigoe T, et al. Immunogenic enhancement and clinical effect by type-I interferon of anti-apoptotic protein, survivin-derived peptide vaccine, in advanced colorectal cancer patients. Cancer Sci. 2011; 102: 1181-7.

[9] Tamura Y, Peng P, Liu K, Daou M, Srivastava PK. Immunotherapy of tumors with autologous tumor-derived heat shock protein preparations. Science. 1997; 278: 117-20.

[10] Udono H, Levey DL, Srivastava PK. Cellular requirements for tumor-specific immunity elicited by heat shock proteins: tumor rejection antigen gp96 primes CD8+ T cells in vivo. Proc Natl Acad Sci U S A. 1994; 91: 3077-81.

[11] Sato K, Torimoto Y, Tamura Y, et al. Immunotherapy using heat-shock protein preparations of leukemia cells after syngeneic bone marrow transplantation in mice. Blood. 2001; 98: 1852-7.

[12] Noessner E, Gastpar R, Milani V, et al. Tumor-derived heat shock protein 70 peptide complexes are cross-presented by human dendritic cells. J Immunol. 2002; 169: 5424-32.

[13] Berwin B, Rosser MF, Brinker KG, Nicchitta CV. Transfer of GRP94(Gp96)-associated peptides onto endosomal MHC class I molecules. Traffic. 2002; 3: 358-66.

[14] Murshid A, Gong J, Calderwood SK. Heat shock protein 90 mediates efficient antigen cross presentation through the scavenger receptor expressed by endothelial cells-I. J Immunol. 2010; 185: 2903-17.

[15] Kleijmeer MJ, Escola JM, UytdeHaag FG, et al. Antigen loading of MHC class I molecules in the endocytic tract. Traffic. 2001; 2: 124-37.

[16] Kutomi G, Tamura Y, Okuya K, et al. Targeting to static endosome is required for efficient cross-presentation of endoplasmic reticulum-resident oxygen-regulated protein 150-peptide complexes. J Immunol. 2009; 183: 5861-9.

[17] Lakadamyali M, Rust MJ, Zhuang X. Ligands for clathrin-mediated endocytosis are differentially sorted into distinct populations of early endosomes. Cell. 2006; 124: 997-1009.

[18] Burgdorf S, Kautz A, Bohnert V, Knolle PA, Kurts C. Distinct pathways of antigen uptake and intracellular routing in CD4 and CD8 T cell activation. Science. 2007; 316: 612-6.

Figure Legends

FIGURE 1. Cross-presentation of Hsp90-chaperoned peptides by human Mo-DCs. (A) Human monocyte-derived DCs ($1x10^5$) were pulsed with Hsp90 (400 μg/ml), precursor peptide survivin-$2B_{75-93}$ (400 μg/ml) alone, a complex of Hsp90 (100 μg/ml or 400 μg/ml) and survivin-$2B_{75-93}$ (100 μg/ml or 400 μg/ml), a simple mixture of both or survivin-$2B_{80-88}$ peptide (for positive control) for 2 h at 37°C and then fixed with 0.01% glutaraldehyde, washed, and cultured with survivin-$2B_{80-88}$-specific CTL clone ($1x10^5$/well). Activation of CTLs was measured as IFN-γ production using ELISA. (B) Mo-DCs ($1 x10^5$) were loaded with various doses of survivin-$2B_{80-88}$ peptide (6, 25, 100, and 400 μg/ml) or Hsp90-survivin-$2B_{75-93}$ precursor peptide complex (6/6, 25/25, 100/100 and 400/400 μg/ml) for 2 h in 100 μl of Opti-MEM and fixed with 0.01% glutaraldehyde. The cells were washed and cultured overnight with $1 x10^5$ survivin-$2B_{80-88}$-specific CTL clone. Activation of CTLs was measured as IFN-γ production using ELISA. Data are shown as means +SEM of three independent experiments. *, $p < 0.01$.

FIGURE 2. Peptide-specific precursor CTLs were activated by cross-presentation of Hsp90-peptide complex. PBMCs were isolated from patient 1 suffering from colon cancer (Table 1) who has been vaccinated with survivin-2B$_{80-88}$ peptide in our clinical study. The patient's PBMCs were shown to contain the survivin-2B-specific CD8^{+} T cells. PBMCs were stimulated with Mo-DCs loaded with survivin-2B$_{80-88}$ (400 μg/ml), Hsp90 (400 μg/ml), survivin-2B$_{75-93}$ precursor peptide (400 μg/ml), and Hsp90 (400 μg/ml)-survivin-2B$_{75-93}$ precursor peptide (400 μg/ml) complex in AIM V medium containing 10% human serum and IL-2 (50 U/ml) for 7 days. The stimulated PBMCs were stained with HIV tetramer or survivin-2B tetramer at 37°C for 20 min. Then a PE-Cy5-conjugated anti-CD8 antibody was added at 4°C for 30 min. Cells were washed twice with PBS. After washing, cells were fixed with 0.5% paraformaldehyde and analyzed by flowcytometry using FACScalibur and CellQuest software (Becton Dickinson, San Jose, California, USA). CD8^{+} living cells were gated, and cells labeled with sirvivin-2B tetramer were referred to as tetramer-positive cells. The frequency of CTL precursors was calculated as the number of tetramer-positive cells divided by the number of CD8^{+} cells. Data are shown as means + SEM of three independent

experiments. *, $p < 0.01$.

FIGURE 3. Memory CD8$^+$ T cells activated by cross-presentation of Hsp90-peptide complex became functional peptide-specific CTLs. CD8-positive T cells separated from patient 1's (Table 1) PBMCs (5 x 10^3 cells/well) were stimulated with Mo-DCs loaded with survivin-2B$_{80-88}$ (400 μg/ml), Hsp90 (400 μg/ml), precursor peptide survivin-2B$_{75-93}$ (400 μg/ml), and Hsp90 (100 μg/ml or 400 μg/ml)-survivin-2B$_{75-93}$ (100 μg/ml or 400 μg/ml) complex, were added to each well along with HLA-A24-transfected T2 (T2-A24) cells (5 x 10^4 cells/well) that had been preincubated with survivin-2B$_{80-88}$ (10 μg/ml) or HIV with an HIV peptide as a negative control. After incubation in a 5% CO_2 humidified chamber at 37° C for 24 h, the wells were washed vigorously five times with PBS and incubated with a biotinylated anti-human IFN-γ antibody and horseradish peroxidase-conjugated avidin. Spots were visualized and analyzed using KS ELISPOT (Carl Zeiss, Jena, Germany). Data are shown as means + SEM of three independent experiments. *, $p < 0.01$.

FIGURE 4. Hsp90-survivn-2B$_{75-93}$ precursor peptide complex localized to static early endosomes within human Mo-DCs. A, Human-Mo-DCs were incubated at 37°C with Alexa 594-labeled Hsp90-survivin-2B$_{75-93}$ peptide complex for 1 h and then washed and fixed. Organelles were stained with an anti-EEA1 mAb for early endosomes, anti-Rab5 pAb for early endosomes, and anti-LAMP-1 pAb for late endosomes/lysosomes followed by Alexa 488-conjugated goat anti-rabbit IgG or anti-mouse IgG and were visualized with confocal laser microscopy. Colocalization of the internalized Hsp90-survivin-2B$_{75-93}$ peptide complex and each organelle is indicated by arrowheads. B, To quantify the percentage of colocalization, a single z-plane of one cell was evaluated. For each protein and organelle combination, a total of 150 cells (50 cells from three independent experiments) were analyzed. Data are shown as means +SEM of three independent experiments. *, $p < 0.01$.

Figure 5. LDL was targeted to the dynamic early endosome followed by translocation to the late endosome/lysosome for degradation. A, Mo-DCs were incubated at 37°C with Alexa 594-labeled LDL. Organelles were stained with an

anti-EEA1 mAb, anti-Rab5 pAb, and anti-LAMP-1 pAb, followed by Alexa 488-conjugated goat anti-rabbit IgG or anti-mouse IgG. Colocalization of internalized LDL and each organelle is indicated by arrowheads. B, To quantify the percentage of colocalization, a single z-plane of one cell was evaluated. For each protein and organelle combination, a total of 150 cells (50 cells from three independent experiments) were analyzed. Data are shown as means +SEM of three independent experiments. *, $p < 0.01$.

Figure 6. Hsp90-peptide complex is cross-presented via an endosome-recycling pathway.

A and B, Mo-DCs were pre-incubated with chloroquine (A) or primaquine (B) at 37°C for 2 h and then loaded with survivin-2B$_{80-88}$ peptide alone or Hsp90-survivin-2B$_{75-93}$ precursor peptide complex for 2 h. The Mo-DCs were then fixed, washed and cultured overnight with survivin-2B$_{80-88}$-specific CTL clone. Activation of CTL was measured as IFN-γ production using ELISA.

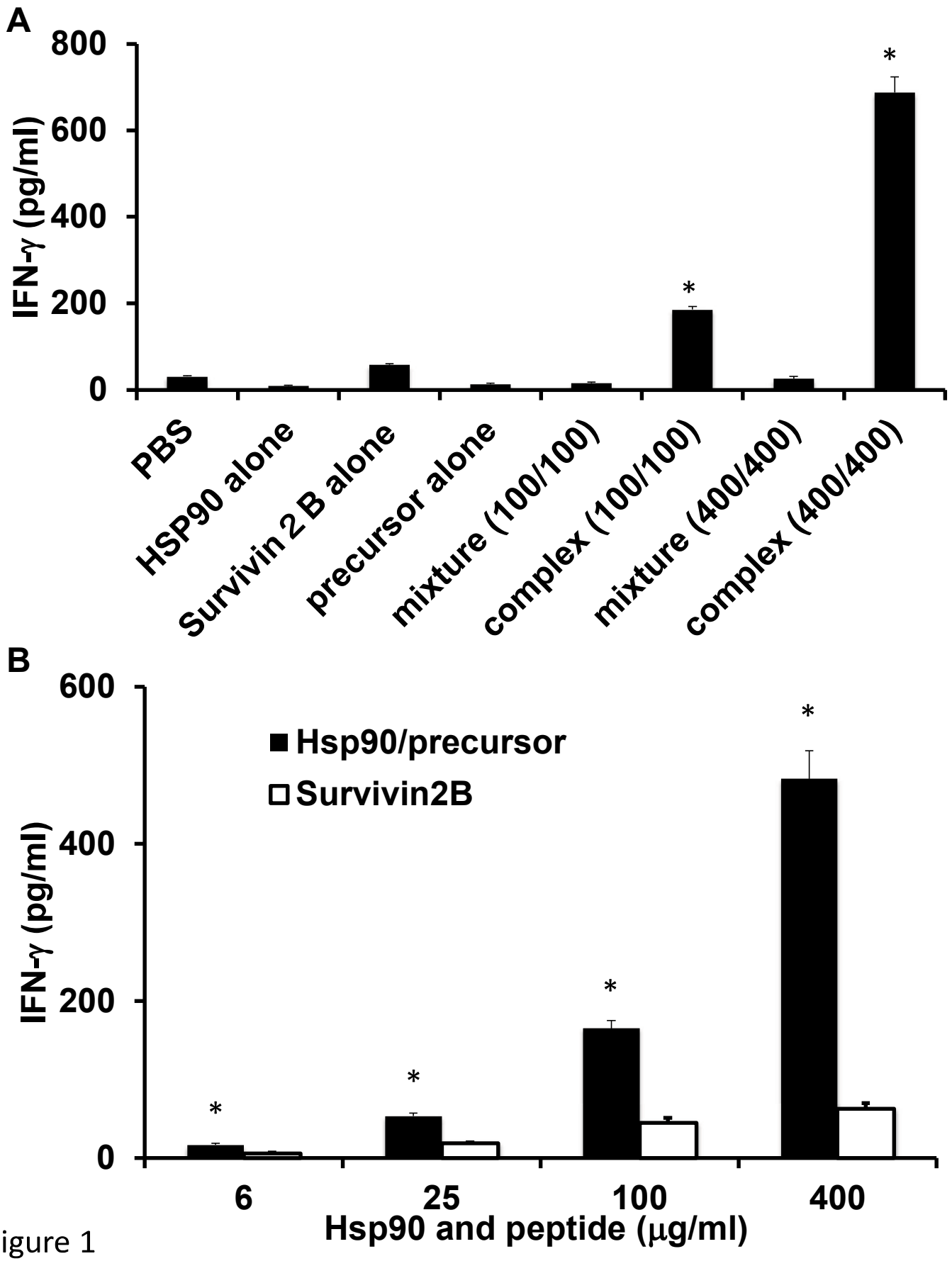
A
800
600
400
200
0
IFN-γ (pg/ml)
*
*
PBS
HSP90 alone
Survivin 2 B alone
precursor alone
mixture (100/100)
complex (100/100)
mixture (400/400)
complex (400/400)
B
600
400
200
0
IFN-γ (pg/ml)
Hsp90/precursor
Survivin2B
*
*
*
*
6
25
100
400
Hsp90 and peptide (μg/ml)

Figure 1

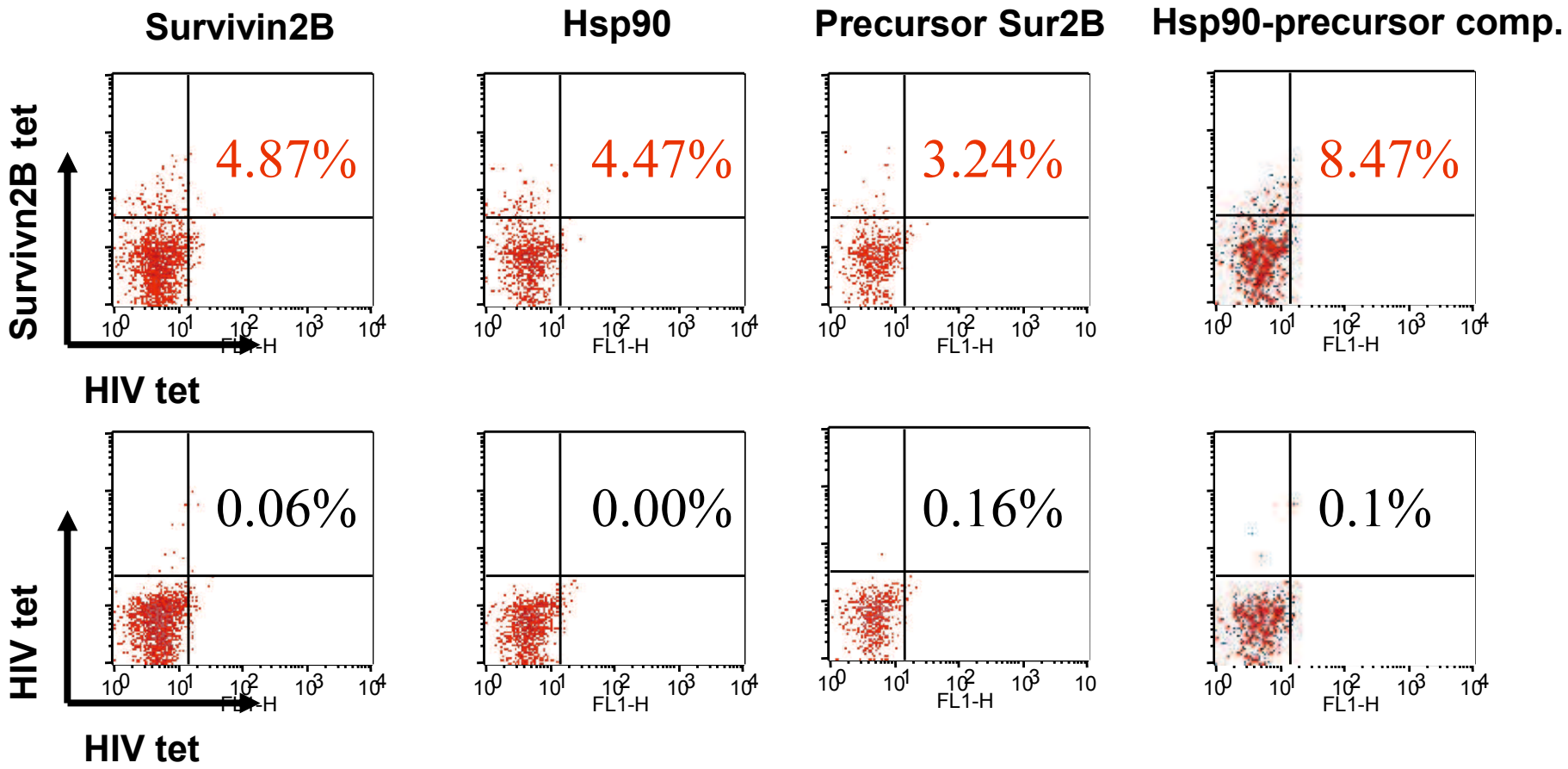
Survivin2B
Hsp90
Precursor Sur2B
Hsp90-precursor comp.
Survivn2B tet
HIV tet
4.87%
4.47%
3.24%
8.47%
0.06%
0.00%
0.16%
0.1%
FL1-H

Figure 2

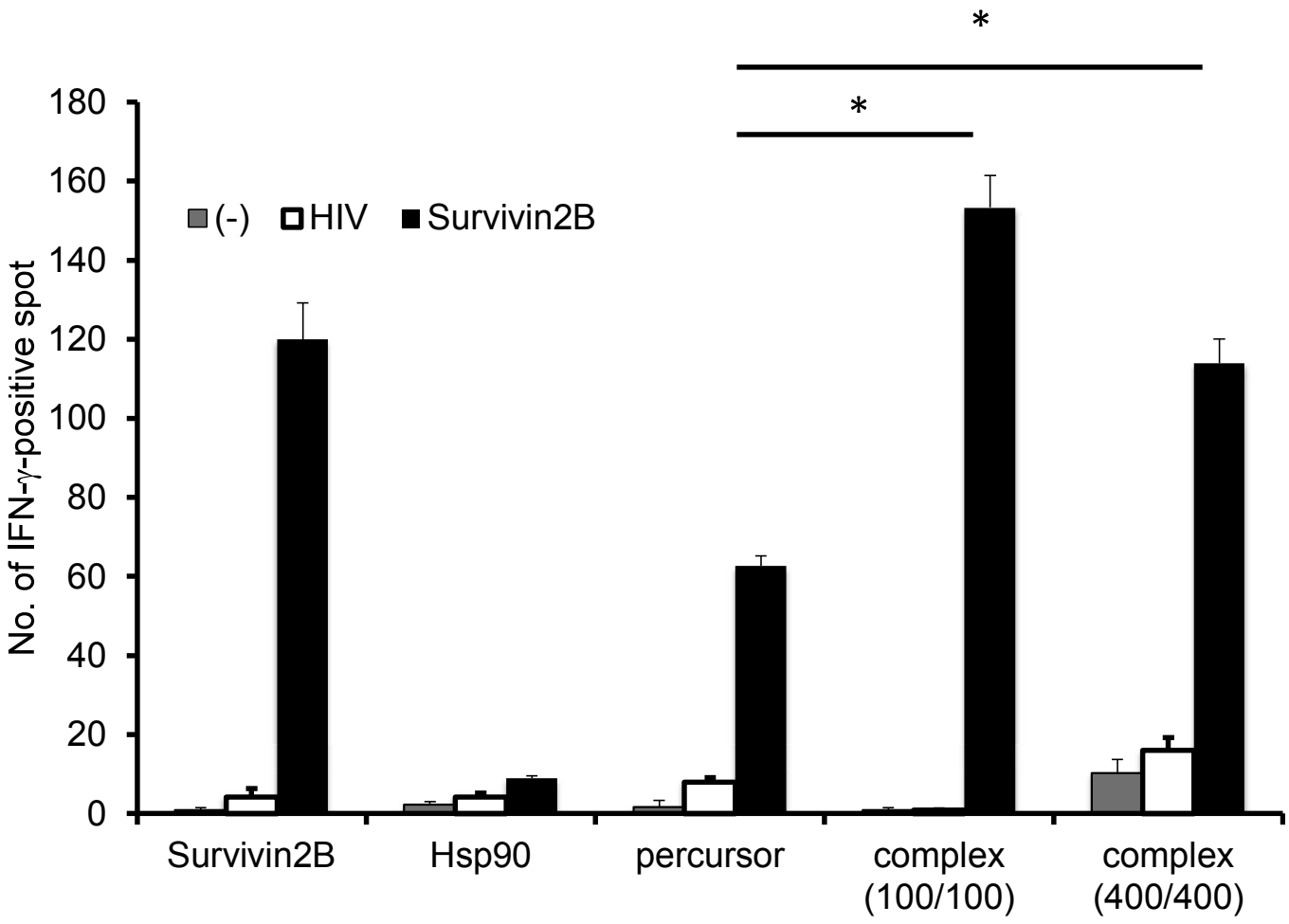
*
*
180
160
140
120
100
80
60
40
20
0
No. of IFN-γ-positive spot
(-)
HIV
Survivin2B
Survivin2B
Hsp90
percursor
complex
(100/100)
complex
(400/400)

Figure 3

A

Hsp90
Rab5

Hsp90
EEA1

Hsp90
LAMP1

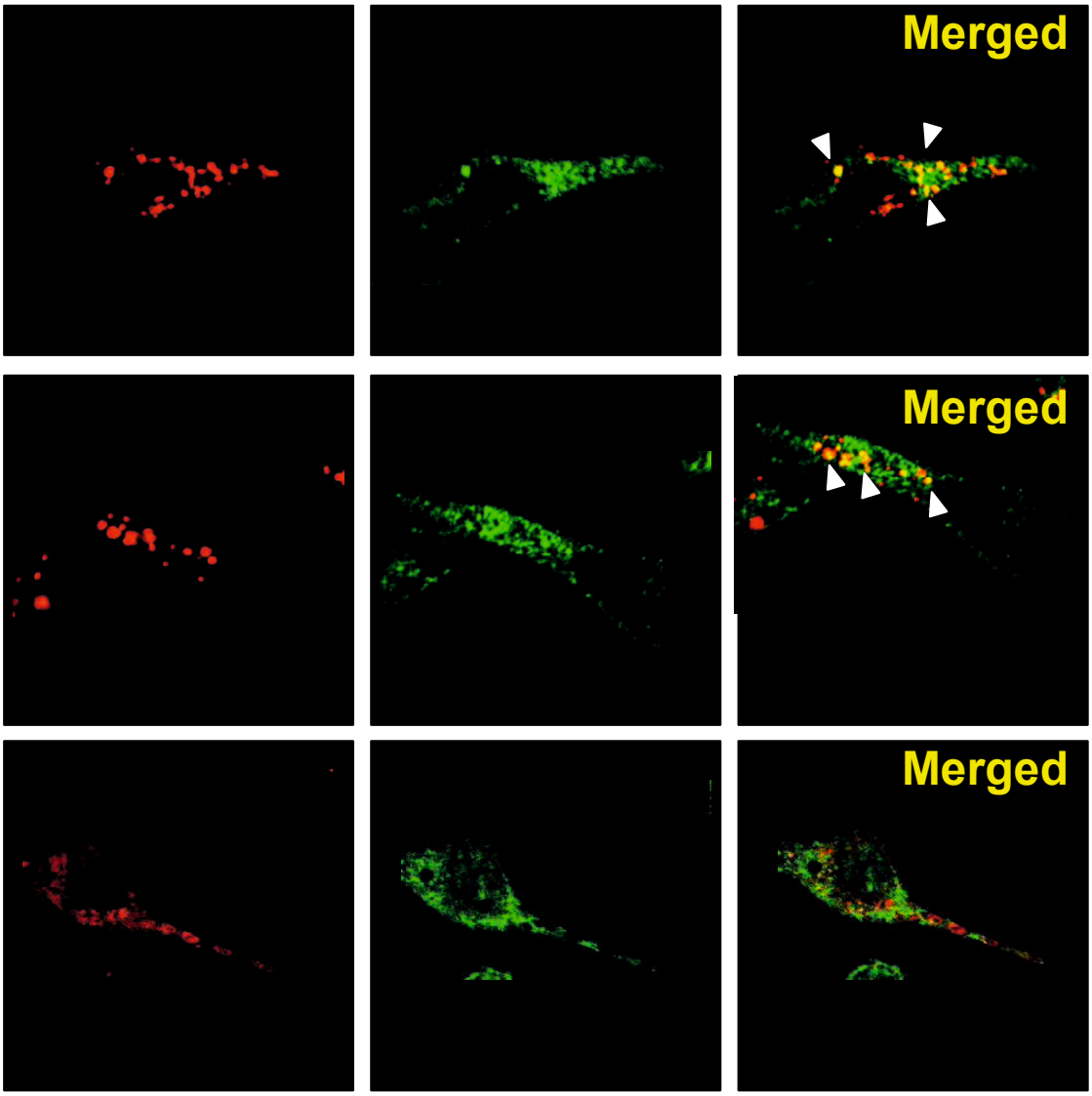

B

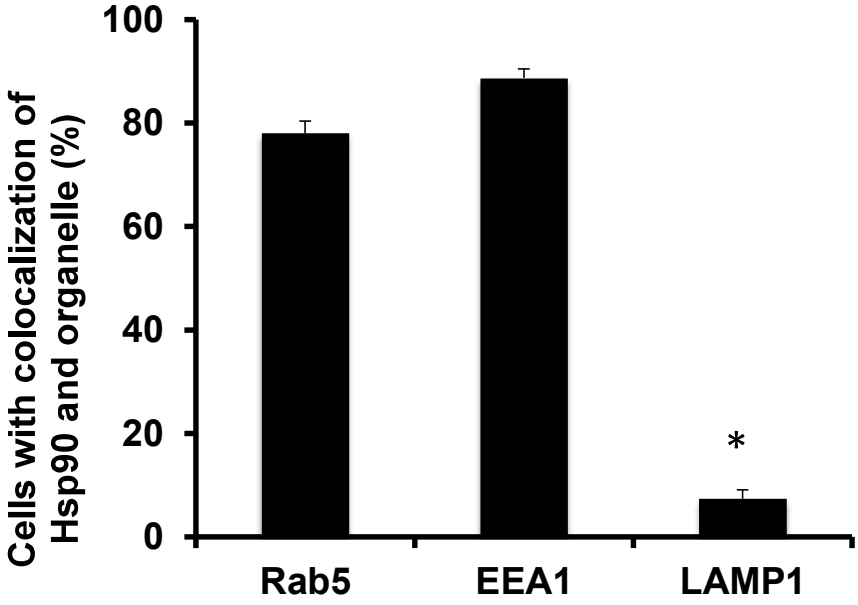

Figure 4

A

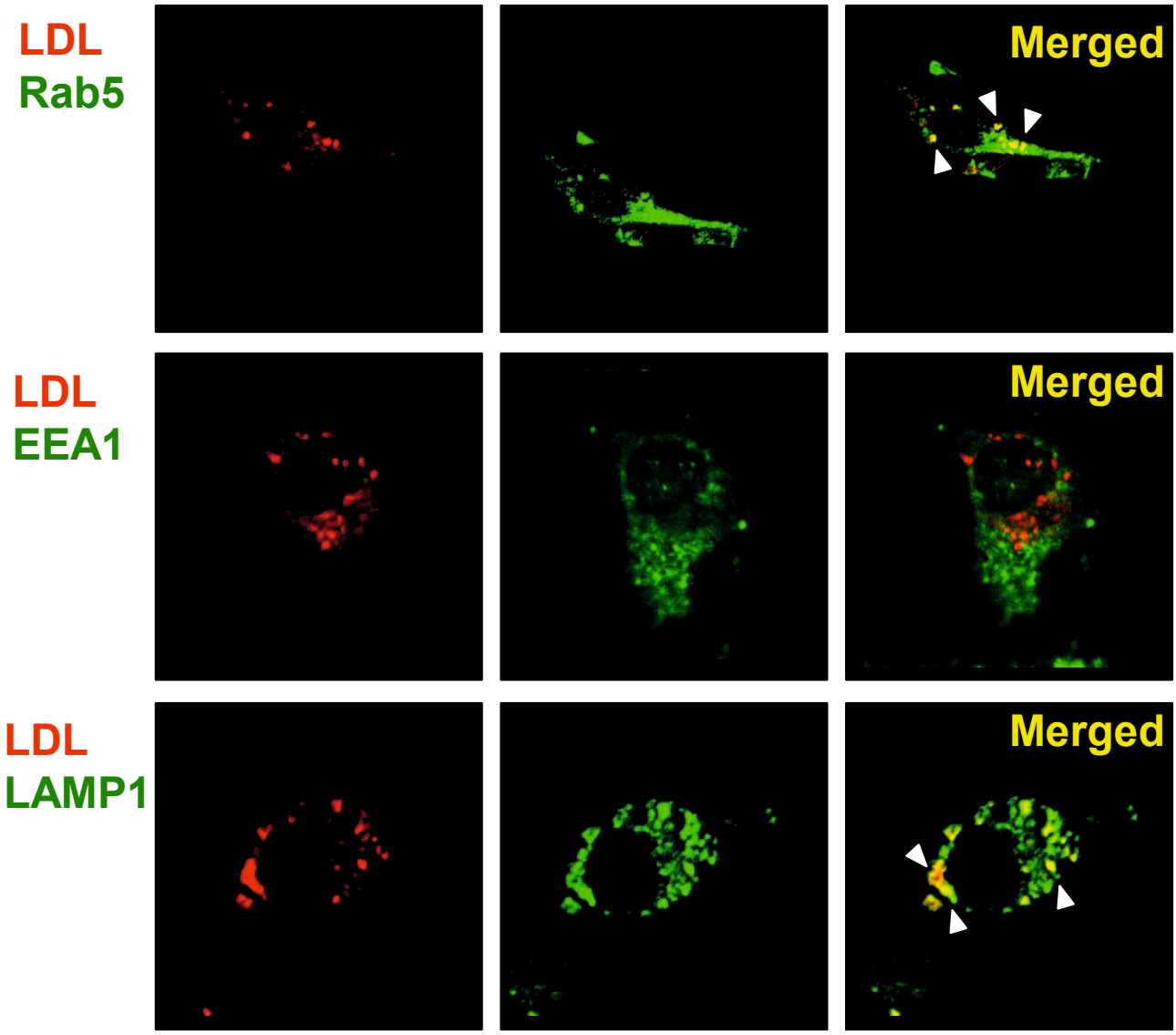
LDL
Rab5
Merged
LDL
EEA1
Merged
LDL
LAMP1
Merged

B

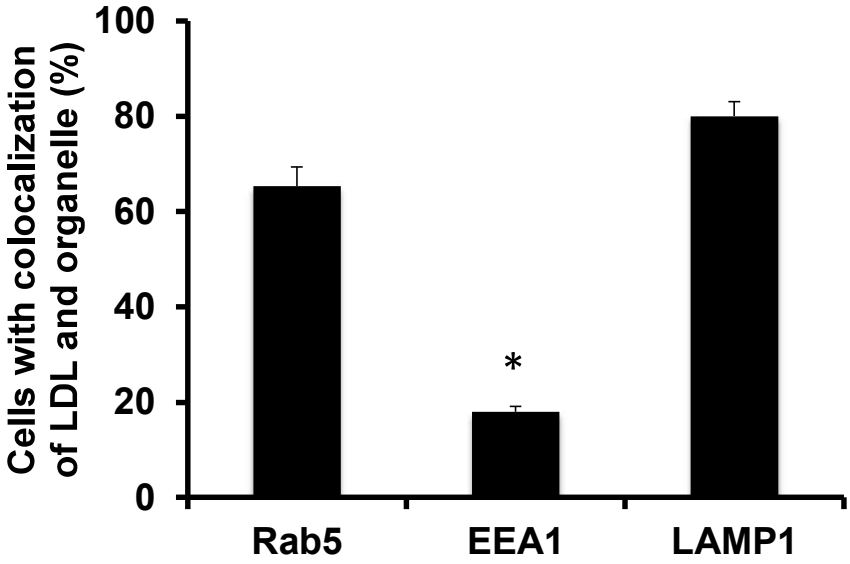
Cells with colocalization of LDL and organelle (%)
100
80
60
40
20
0
*
Rab5
EEA1
LAMP1

Figure 5

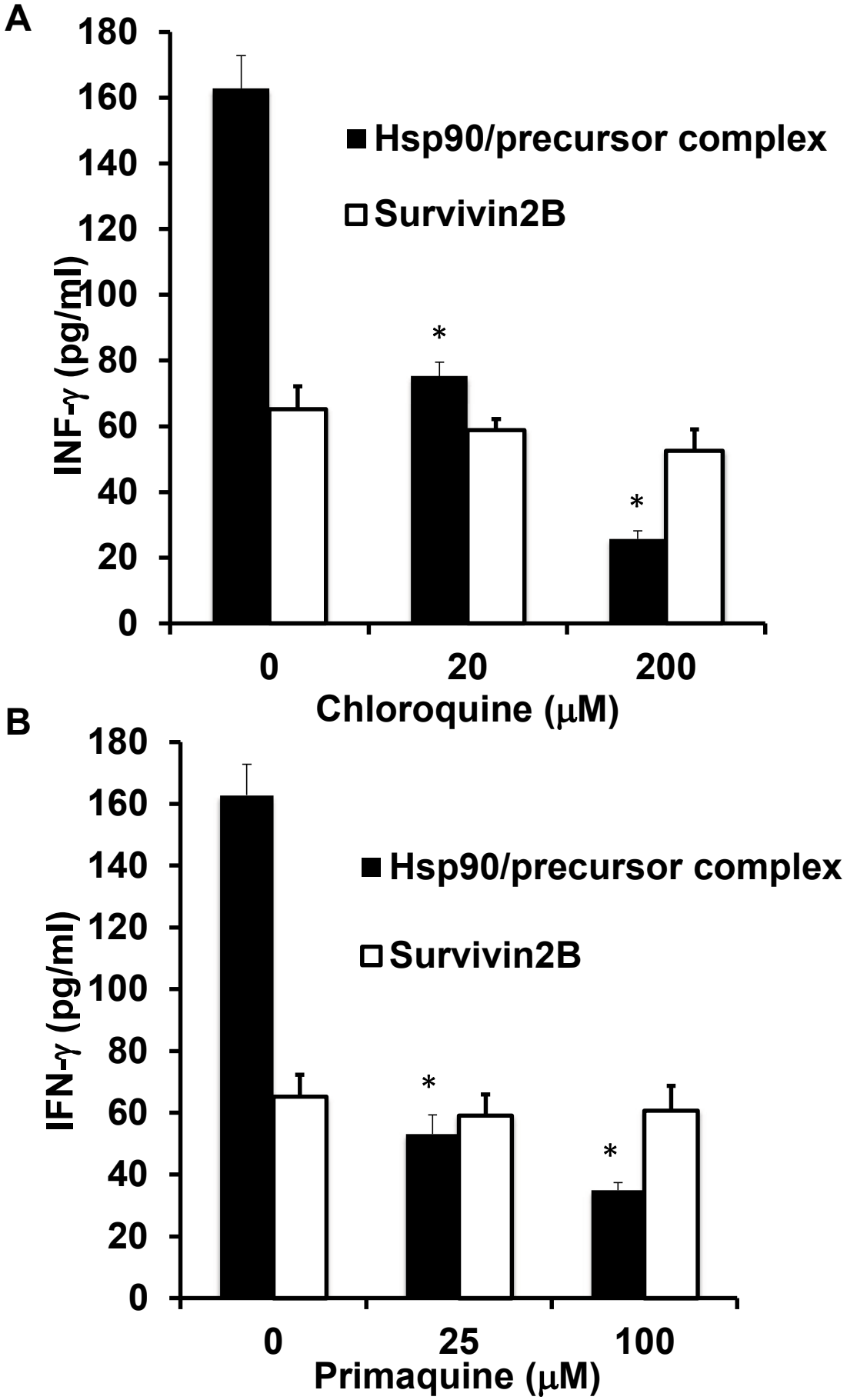
A
180
160
140
120
100
80
60
40
20
0
INF-γ (pg/ml)
Hsp90/precursor complex
Survivin2B
*
*
0
20
200
Chloroquine (μM)
B
180
160
140
120
100
80
60
40
20
0
IFN-γ (pg/ml)
Hsp90/precursor complex
Survivin2B
*
*
0
25
100
Primaquine (μM)

Figure 6

Table 1. Quantitation of survivin-2B-specific CD8 T cells by tetramer assay

Patient no.	Tumor	Survivin-2B80-88-specific CD8 T cell frequency (tetramer staining)					Effect
		in vitro stimulation	(-)	survivin-2B80-88	Hsp90	survivin-2B75-93	Hsp90-survivin-2B75-93	
1	Colon	0.06	4.87	4.47	3.24	**8.47**	**
2	Colon	0.32	2.87	0.77	4.01	1.30	
3	Pancreas	0.70	6.27	1.70	1.88	**6.64**	**
4	Pancreas	0.48	4.56	0.84	1.28	**3.02**	*
5	ampulla of Vater	1.27	4.60	0.97	2.24	**6.50**	**
6	Breast	3.59	3.78	3.00	3.06	**3.82**	**
7	Breast	3.98	3.91	1.94	2.28	**6.19**	**
8	Breast	2.76	3.92	2.91	2.08	**6.07**	**

*Frequency of survivin-2B-specific CD8 T cell stimulated with Hsp90-survivin-2B75-93 peptide complex was increased compared with stimulation with survivin-2B75-93 precursor peptide
** Frequency of survivn-2B-specific CD8 T cell stimulated with hsp90-survivin-2B75-93 peptide was increased compared with stimulation with both survivin-2B80-88 peptide and survivin-2B75-93 peptide.

Chapter II

Cancer-associated oxidoreductase ERO1-α drives the production of tumor-promoting myeloid-derived suppressor cells via oxidative protein folding.

Abstract

Endoplasmic reticulum (ER) disulfide oxidase ERO1-α plays a role in the formation of disulfide bonds in collaboration with PDI. The disulfide bond formation is required for the proper conformation and function of secreted and cell surface proteins. We found that ERO1-α was overexpressed in a variety of tumor types. Therefore, we examined the role of ERO1-α in tumor growth. In BALB/c mice, knockdown of ERO1-α within 4T1 mouse mammary gland cancer cells (KD) caused retardation of *in vivo* tumor growth compared with tumor growth of scrambled control cells (SCR). In contrast, when ERO1-α-overexpressed 4T1 cells (OE) were compared with mock control cells (mock), OE showed augmented tumor growth compared with mock.

However, differences of tumor growth were not observed among four groups of nude mice, suggesting that expression of ERO1-α diminished antitumor immunity. We observed dense peritumoral granulocytic infiltrates in tumors of wild-type 4T1 and SCR but not KD, and these cells were identified as polymorphonuclear myeloid-derived suppressor cells (PMN-MDSCs). In addition, production of G-CSF and CXCL1/2, which have intramolecular disulfide bonds, from KD was significantly decreased compared with that from SCR. In contrast, OE produced a larger amount of these molecules that did mock. These changes were regulated at the post-transcriptional level. These results suggest that overexpression of ERO1-α in the tumor inhibits T cell response by recruiting PMN-MDSCs via regulation of MDSC-prone cytokines and chemokines.

1. Introduction

The tumor microenvironment has been shown to be an immunosuppressive microenvironment. Myeloid-derived suppressor cells (MDSCs) are a major component of the immune-suppressive network in cancer and many other pathological conditions.

Experimental models using mice have shown that MDSCs can facilitate tumor progression by promoting the suppression of antitumor immunity[1-4], promoting inflammation[4, 5], stimulating angiogenesis[6], and enhancing tumor cell migration and metastasis[7]. Clinical studies have further demonstrated that the presence of MDSCs correlates with adverse outcomes and shorter survival in various types of cancer, including breast cancer[8]. MDSCs are a heterogeneous group of myeloid cells characterized by potent immunosuppressive activity. In mice, they are characterized as $CD11b^{+}$ $Gr\text{-}1^{+}$ cells. In recent years, two major groups of cells that comprise MDSCs have been identified: cells with morphology and phenotype ($CD11b^{+}$ $Ly6C^{low}$ $Ly6G^{+}$) typical of polymorphonuclear-PMN-MDSCs and cells with morphology and phenotype ($CD11b^{+}$ $Ly6C^{high}$ $Ly6G^{-}$) typical of monocytes-Mo-MDSCs. Mo-MDSCs consist of immature myeloid cells with the ability to differentiate to macrophages and DCs. PMN-MDSCs are the largest population of MDSCs in tumor-bearing mice, representing >75% of all MDSCs. They suppress antigen-specific T cell response, primarily via release of ROS. PMN-MDSCs have also been found in cancer patients. Thus, PMN-MDSCs play a pivotal role in tumor progression. However, the underlying

mechanism by which PMN-MDSCs proliferate and infiltrate into tumor sites has been unclear. G-CSF is a cytokine with potent neutrophil proliferation activity. G-CSF is produced by macrophages, fibroblasts and endothelial cells. Recently, it has been shown that tumor cells are a source of G-CSF[9-12] and that production of G-CSF by tumors is responsible for the recruitment of immunosuppressive PMN-MDSCs, which promote tumor growth via inhibition of antitumor immune responses[13, 14]. A vital role of tumor-derived G-CSF in tumor bearing mice was demonstrated by Waight et al.[13] In addition, depletion of G-CSF resulted in reduced tumor growth in a murine mammary gland cancer 4T1 model. 4T1 cells were previously shown to express a G-CSF transcript. Thus, G-CSF is a candidate molecular target of cancer treatment.

ERO1-α is an ER-resident oxidase. ERO1-α and PDI play a central role in disulfide bond formation of secreted and cell surface molecules[15-18]. Disulfide bond formation, i.e., oxidative protein folding, is the most common post-translational modification and is required for proper conformation and function of these molecules. Thus, these secreted and cell surface molecules need to be regulated by not only the gene expression level but also proper post-transcriptional modification. We have

recently demonstrated that various types of tumor cells expressed high levels of ERO1-α and that ERO1-α is a poor prognostic marker for breast cancer[19]. Here we demonstrate that ERO1-α plays a pivotal role in PMN-MDSCS induction via upregulation of G-CSF production from cancer cells in collaboration with PDI.

2. Materials and methods

2.1 Cells

The murine breast cancer cell line 4T1 and human breast cancer lines MCF7, BT-474, UACC-893, SK-BR-3, MDA-MB-157, MDA-MB-231, MDA-MB-468 were purchased from ATCC (Manassas, VA, USA). 4T1, BT-474 and MDA-MB-157 cells were cultured in RPMI-1640 (Sigma-Aldrich, St. Louis, MO, USA), MCF7, MDA-MB-231 and MDA-MB-468 cells were cultured in Dulbecco's modified Eagle's medium (Sigma-Aldrich), UACC-893 cells were cultured in Leibovitz's L-15 (Life Technologies, Carlsbad, CA, USA) and SK-BR-3 cells were cultured in McCoy's 5A media (Life Technologies) supplemented with 10% FCS at 37℃ in 5% CO_2. Short hairpin RNA for murine ERO1-α (TR502816) was purchased from OriGene (Rockville,

MD, USA) and transfected to 4T1 cells using Lipofectamine RNAiMAX (Life Technologies). Cells were stably propagated under puromycin selection (6 μg/ml). The murine ERO1-α gene fragment was isolated from pCMV6-Entry Vector/mERO1-α (OriGene) digested with BamH1 and Xho I, and then inserted into an appropriate site of the expression vector pcDNA6/myc-HisA (Invitrogen, Carlsbad, CA, USA). The resulting pcDNA6/mERO1-α or an empty vector as a control was transfected into 4T1 cells using Lipofectamine 2000 (Life Technologies). Cells were stably propagated under blasticidin (5 μg/ml, Life Technologies) selection.

2.2 In vivo study

Female BALB/c and BALB/c nu/nu mice, 4 weeks old, were obtained from the Jackson Laboratory (Bar Harbor, ME, USA) and used at 5 weeks of age. Mice were maintained in a specific pathogen-free mouse facility at Sapporo Medical University (Sapporo, Japan) according to institutional guidelines for animal use and care. For tumor formation studies, mice were injected with 3×10^4 4T1 cells, ERO1-α-overexpressed cells (OE) or ERO1-α knockdown cells (KD) into the right 4th mammary

glands. Tumor growth was measured 2-3 times/week in two dimensions, and tumor volume was calculated using the formula 3.14 x (width^2 x length)/6. Tumor length and width were measured with a caliper.

2.3 Treatments

Mice were challenged with 3×10^4 4T1 SCR cells. For the depletion of CD4$^+$ and/or CD8$^+$ T cells, mice were injected intraperitoneally with a CD4-specific antibody and/or CD8-specific antibody at 200 μg/mouse on day 3 before and day 1 after tumor challenge. For depletion of Ly6G$^+$ PMN-MDSCs, mice were injected intraperitoneally with Ly6G-specific antibody clone 1A8 (Bio X Cell, West Lebanon, NH, USA) or Rat IgG (Sigma-Aldrich) at 100 μg/mouse every 2 days from day 15 after the tumor challenge.

2.4 Quantitative reverse transcription-PCR (qPCR) analysis and real-time PCR

Total RNA was isolated from cultured cells and normal breast tissues using Isogen reagent (Nippon Gene, Tokyo, Japan) and RNeasy Mini kits (QIAGEN, Valencia, CA)

according to manufacturer's instructions. The cDNA mixture was synthesized from 1 μg total RNA by reverse transcription using Superscript III and oligo (dT) primer (Life Technologies) according to the manufacturer's protocol. PCR amplification was performed in 20 μl of PCR mixture containing 1 μl of cDNA mixture, 0.1 μl of Taq DNA polymerase (QIAGEN) and 6 pmol of primers. Real time-relative quantitative polymerase chain reaction (qPCR) was performed with a QuantiTect SYBR Green PCR Kit (QIAGEN) to determine the expression levels of cxcl1, cxcl2, g-csf and β-actin. Expression values for each sample were normalized to β-actin, and fold levels of the indicated genes represent the mean (±SEM) of replicate reactions. Primer sequences were as follows: β-actin (actb), QuantiTect Mm Actb 1 SG Primer Assay; cxcl1, QuantiTect Mm_Cxcl1_1_SG Primer Assay; cxcl2, QuantiTect Mm_Cxcl2_1_SG; g-csf (Csf3), QuantiTect Mm_Csf3_1_SG (QIAGEN). PCR cycles were performed on the StepOne Real-Time PCR System (Life Technologies) with the following cycle conditions: 10 min at 95°C, 45 cycles of 15 s at 95°C and 1 min at 60°C, followed by melting curve analysis. The delta-delta Ct method was used for data analysis.

Real time-relative polymerase chain reaction (real-time PCR) was performed to

determine the expression levels of ERO1-α and β-actin. Expression values for each sample were normalized to β-actin, and fold levels of the indicated genes represent the mean (±SEM) of replicate reactions. Primer sequences were as follows: β-actin (ACTB), Hs0160665_g1; ERO1-α (ERO1L), Hs00205880_m1 (Life Technologies). PCR cycles were performed on the StepOne Real-Time PCR System (Life Technologies) with the following cycle conditions: 2 min at 50 °C, 10 min at 95°C, 40 cycles of 15 s at 95°C and 1 min at 60°C. The delta-delta Ct method was used for data analysis.

2.5 Western blot analysis.

Cultured cells were washed in ice-cold PBS, lysed by incubation on ice in a lysis buffer (50 mmol/L Tris-HCl [pH 7.5, 150 mmol/L NaCl, 5 mmol/L EDTA, 1% NP40], and cleared by centrifugation at 21880g for 30 min at 4°C. For blockade of free thiols, cells were pretreated for 5 min with 10 mM methyl methanethiosulfonate (Pierce, Rockford, IL, USA) in PBS. Post-nuclear supernatants were divided and heated for 5 min at 95°C in a non-reducing or reducing SDS sample buffer, resolved by SDS-PAGE, and electrophoretically transferred to PVDF membranes (Immobilon-P; Millipore,

Billerica, MA, USA). The membranes were incubated with blocking buffer (5% non-fat dried milk in PBS) for 30 min at room temperature and then incubated overnight with anti-ERO1-α mAb (Abnova, Taipei, Taiwan), anti-PDI polyclonal antibody (Enzo Life Sciences, Farmingdale, NY, USA), anti-mG-CSF (R&D Systems, Minneapolis, MN, USA), or mouse anti-β-actin mAb AC-15 (Sigma-Aldrich, St. Louis, MO, USA). After washing three times with wash buffer (0.1% Tween-20 in TBS), the membranes were reacted with peroxidase-labeled goat anti-rabbit IgG antibody, peroxidase-labeled goat anti-mouse IgG antibody or peroxidase-labeled rabbit anti-goat antibody (KPL, Gaithersburg, MD, USA) for 3 h. Finally, the signal was visualized using an ECL detection system (Amersham Life Science, Arlington Heights, IL, USA) or IMMOBILON detection system (Millipore Corporation, Billerica, Massachusetts, USA) according to the manufacturers' protocols.

2.6 Analyses of leukocytic infiltrates in the tumor and flow cytometry

Mice were injected with 1×10^5 4T1 cells, ERO1-α-overexpressed cells or ERO1-α knockdown cells into the right 4th mammary glands. Tumor tissues, peripheral blood,

spleen and bone marrow were collected on day 14 after the tumor challenge. For analyses of leukocytic infiltrates in the tumor tissue, tumors were mechanically dissociated on a wire mesh by crushing with scissors and digested for 2 to 3 h at 37 °C in RPMI medium supplemented with 5% fetal bovine serum and Liberase (Roche, Tokyo, Japan) (1 mg/ml). Then leukocytes were collected by density-gradient centrifugation with lympholyte-M. Peripheral blood, spleen cells and bone marrow were hemolyzed by a hemolytic agent. The cells were filtered through 70 μm nylon strainers (BD Biosciences, Bedford, MA) and counted the cell number. They were then stained with specific markers, and analyzed by flow cytometry. All preparations were pre-incubated with anti-CD16/32 mAb (BD Biosciences, San Diego, CA) to block Fc receptor binding, followed by incubation with a directly conjugated primary antibody. Labeled cells were analyzed by a FACSCalibur flow cytometer (BD, San Jose, CA) and FlowJo (Tree Star Inc., Oregon, USA). Antibodies reactive against the following cell surface markers were used (including appropriate isotype controls): PE-labeled CD11b, PerCP/Cy5.5-labeled Ly6G and APC-labeled Ly6C (BioLegend, San Diego, CA) and PerCP/Cy5.5-labeled Gr-1 (eBioscience, San Diego, CA).

2.7 Immunohistochemistry

Tissue was fixed in neutral 10% buffered formaldehyde, embedded in paraffin, and cut into 5-μm-thick slices for ERO1-α staining. Reactivity of the anti-ERO1-α monoclonal antibody was determined by perinuclear staining within tumor cells, indicating endoplasmic reticulum localization. Tissues were frozen with OCT compound (Leica Biosystems, Nussloch, Germany) and cut into 7-μm-thick slices for CD11b and Gr-1 staining. Antibodies reactive against CD11b and Gr-1 were purchased from BioLegend and eBioscience, respectively. Secondary antibodies were purchased from DAKO Japan (Tokyo, Japan). Tissue sections were developed using a diaminobenzidine. Images were quantified by counting the number of positively stained cells in five randomly selected fields at × 200 magnification.

2.8 Enzyme-linked immunosorbent assay (ELISA).

4T1 cells were plated at 1×10^5 cells／well in 6-well plates for 24 h or 48 h. All samples were stored at -80°C until assayed. Supernatants were diluted and mouse

CXCL-1 (GRO/KC) (IBL, Gunma, Japan), mouse CXCL-2 (MIP-2α) and mouse G-CSF (R&D Systems, Minneapolis, MN, USA) levels were measured using a sandwich ELISA kit. Absorbance was determined at 450 nm.

2.9 Statistical analysis

Student's t-test was used for analysis of two unpaired samples. Statistical differences in results of the study with depletion of $CD4^+$ and/or CD8 T^+ cells were analyzed by Dunnett's test. Differences in the results of the study with depletion of $Ly6G^+$ PMN-MDSCs were assessed by the Mann-Whitney test. Overall survival rates were calculated by the Kaplan–Meier method, and differences in survival curves were assessed by the log–rank test. All analyses were carried out with STATMATE version 3.19 (ATMS Co., Ltd., Tokyo, Japan). A P-value of less than 0.05 was regarded as statistically significant. All statistical tests were two-sided.

3. Results

3.1 Expression of ERO1-α in breast cancer cell lines and breast cancer tissues.

We have shown that ERO1-α expression was augmented in human breast cancer cell lines and breast cancer tissues[19]. Here we showed the expression of ERO1-α on breast cancer cell lines was upregulated regardless of the histological type compared with the expression in normal breast tissues at the mRNA level (Fig. 1A). Immunohistochemical staining also showed that ERO1-α was preferentially expressed within tumor cells but not normal breast tissue (Fig. 1B, 1C). Our previous study demonstrated that none of the normal breast tissues (71 cases) were positive for ERO1-α staining[19].We have observed that ERO1-α showed a patchy staining pattern within cancer nests. As it has been demonstrated that ERO1-α is induced under the condition of hypoxia, we assumed that cancer cells residing within hypoxic areas show augmented expression of ERO1-α. Thus, heterogeneity of ERO1-α expression seems to be attributed to the oxygen and blood supply.

3.2 Knockdown of ERO1-α by shRNA reduced tumor growth via restoration of antitumor T-cell-mediated immunity.

To examine the role of ERO1-α in tumor growth, we generated ERO1-α

knockdown cells (KD) using shRNA against ERO1-α (Fig. 2A). KD cells did not show differences in a proliferation assay compared with wild-type 4T1 (WT) cells and scrambled shRNA-transfected (SCR) cells (Supplemental Fig. 1). When BALB/c nu/nu mice were challenged with SCR cells and KD cells, we observed that these two cell lines grew aggressively at similar growth speeds (Fig. 2B). In contrast, knockdown of ERO1-α caused retardation of tumor growth compared with WT cells in BALB/c mice (Fig. 2C). Knockdown of ERO1-α also had a survival benefit compared with SCR cells (Fig. 2D). These results suggested that ERO1-α (+) WT or SCR tumor cells inhibited antitumor immunity. In other words, depletion of ERO1-α within tumor cells might restore antitumor immunity. To clarify this, we performed a T-cell depletion assay *in vivo*. When $CD4^+$ and/or $CD8^+$ T cells were depleted during tumor growth assay using KD cells, these cells showed tumor growth similar to that of SCR cells, indicating that both $CD4^+$ and $CD8^+$ T cells were responsible for the immunogenicity of KD tumor cells (Fig. 3A). Moreover, since some of the mice challenged with KD cells rejected the tumors, we rechallenged these mice with 4T1 WT cells. All of the mice rechallenged with 4T1 tumor cells rejected tumor cells (Fig. 3B), indicating that KD tumor cells

acted as immunogenic tumor cells due to ERO1-α knockdown. Based on these results, both $CD4^+$ and $CD8^+$ T-cell-mediated antitumor immunity against 4T1 tumor was dampened by the expression of ERO1-α within 4T1 tumor cells.

3.3 Enhanced expression of ERO1-α promotes the tumor growth *in vivo* via suppression of antitumor immunity.

To further confirm the effect of ERO1-α on tumor growth and antitumor immunity, we generated an ERO1-α-overexpressed 4T1 cell line (OE) by introducing murine cDNA of ERO1-α (Fig. 4A). When 4T1 cells transfected with a control vector (mock) and OE cells were inoculated to nude mice, there was no difference in tumor growth rates (Fig. 4B), but, when they were inoculated to BALB/c WT mice, OE tumors grew more aggressively than did mock cell tumors (Fig. 4C, 4D). These results again suggested that expression of ERO1-α suppressed antitumor immunity against the 4T1 tumor.

3.4 PMN-MDSCs accumulate in the spleen, bone marrow, peripheral blood, and tumor

of ERO1-α (+) 4T1 tumor-bearing mice.

Histopathological findings revealed that ERO1-α (+) SCR 4T1 tumor tissues had a large amount of granulocyte infiltrates in the peritumor site as well as within the tumor mass (Fig. 5A). In clear contrast, KD tumors showed less granulocyte infiltrates (Fig. 5B). We compared peritumoral and intratumoral infiltrating cells in SCR and KD tumors by immunohistochemical analysis using CD11b mAb and Gr-1 mAb. Although we observed that the major component was $CD11b^+$ $Gr\text{-}1^+$ MDSCs both in ERO1-α (+) SCR tumors and KD tumors, total numbers of both $CD11b^+$ cells and $Gr\text{-}1^+$ cells were increased in SCR tumors (Fig. 5C, 5E, 5G) compared with those in KD tumors (Fig. 5D, 5F, 5H). Furthermore, we investigated the population of these infiltrates using a flow cytometer. Interestingly, $Ly6G^+$ polymorphonuclear MDSCs (PMN-MDSCs) were predominantly observed in the spleen (40.9% vs 17.2%), bone marrow (67.0% vs 57.7%), peripheral blood (57.6% vs 23.7%), and tumor (45.2% vs 27.9%) in SCR tumor-bearing mice compared with those in KD tumor-bearing mice (Fig.6A, 6B, 6C, 6D and supplemental Table 1A). In contrast, when we compared mice bearing mock tumors and OE tumors, we observed that PMN-MDSC infiltration was higher in OE

tumor-bearing mice than that in mock-bearing mice in the spleen (31.0% vs 18.1%), bone marrow (61.6% vs 60.4%), peripheral blood (50.3% vs 22.3%), and tumor (49.5% vs 37.6%) (Fig. 7A, 7B, 7C, 7D and supplemental Table 1B). These results suggested that the expression of ERO1-α within the tumor resulted in accumulation of PMN-MDSC throughout the body including the spleen, bone marrow, peripheral blood as well as the tumor, leading to the suppression of antitumor T-cell-mediated immunity by PMN-MDSCs.

3.5 Depletion of $Ly6G^+$ PMN-MDSCs renders tumor cells immunogenic.

To determine whether $Ly6G^+$ MDSCs were the main immunosuppressor cells in the 4T1 tumor system, we depleted $Ly6G^+$ cells during the tumor growth assay using anti Ly6G mAb (1A8). Although depletion of $Ly6G^+$ cells seemed incomplete, about 50% of $Ly6G^+$ cells remained in the peripheral blood (supplemental Fig.2), apparently, depletion of $Ly6G^+$ cells retarded SCR tumor growth compared with the growth of isotype-matched control IgG-treated tumors, and SCR tumor growth was almost the same as tumor growth in mice challenged with KD cells (Fig. 8). These results indicated

that (tumor-associated) Ly6G^{+} PMN-MDSCs were the main immunosupressor cells for ERO1-α (+) 4T1 tumor cells.

3.6 Tumor ERO1-α plays a crucial role in the induction and recruitment of PMN-MDSCs.

We examined the mechanism of induction of tumor-associated PMN-MDSCs.

Since it was demonstrated that G-CSF and GM-CSF induce proliferation of PMN-MDSCs[1, 13, 14], we measured the production G-CSF and GM-CSF from 4T1 tumor cells using ELISA. We found that ERO1 (+) SCR cells produced a large amount of G-CSF compared with the amount produced by the KD cells (Fig. 9A). In addition, albeit to the lesser extent, production of GM-CSF from SCR cells was shown to be greater than that from KD cells (supplemental Fig. 3A). Whereas G-CSF amplifies PMN-MDSCs in the spleen, bone marrow and peripheral blood, PMN-MDSCS recruitment from the circulation to tumor stroma is thought to occur mainly via interaction between the chemokines CXCL1 and CXCL2[20, 21] and their receptor CXCR2 expressed on PMN-MDSCs[20]. Therefore, we compared the concentrations of CXCL1

and CXCL2 in the culture supernatant of each cell line. SCR cells produced a larger amount of CXCL1 and CXCL2 for PMN-MDSCS recruitment than did KD cells (Fig. 9B, 9C). In contrast, when we compared mock cells and OE cells, OE cells showed greater production of G-CSF, CXCL1, and CXCL2 than did mock (Fig. 9D, 9E, 9F). As expectedly, PMN-MDSCs in the spleen, bone marrow and peripheral blood expressed CXCR2 (supplemental Fig. 3B). These results suggested that tumor-derived G-CSF induced proliferation of PMN-MDSCs followed by recruitment to the tumor sites by augmented production of CXCL1 and CXCL2, resulting in the inhibition of antitumor T-cell-mediated immune response.

3.6 Tumor ERO1-α facilitates the production of G-CSF and CXCL1 and 2 via oxidative folding at the post-transcriptional level.

We investigated the role of ERO1-α in the augmented production of G-CSF, CXCL1, and CXCL2. To determine whether the gene expression level was affected by ERO1-α, we compared the *g-csf* mRNA expression levels by real-time RT-PCR. The mRNA expression levels were not different in mock cells and OE cells, indicating that

the expression of ERO1-α did not influence the *g-csf* gene expression level (Fig. 10A). In addition, we observed that the gene expression levels of *cxcl1* and *cxcl2* were not altered (Fig. 10A). Next, we compared the protein levels using Western blot analysis. Since ERO1-α is known to act as an oxidoreductase, we further investigated the redox states of G-CSF in mock cells and OE cells by Western blot analysis under a non-reducing condition using MMTS. We found that the total amount of G-CSF protein in OE cells was larger than that in mock cells under a reducing condition (Fig. 10B). Moreover, we found that ratio of the oxidized form (mature form) to the reduced form (immature form) of G-CSF in OE cells was much higher than that in mock cells under a non-reducing condition (Fig. 10B). It has been shown that G-CSF has two intramolecular disulfide bonds[22] and that the disulfide bond formation is required for G-CSF to exert its biological activity. Taking this into account, these results indicated that tumor ERO1-α plays a pivotal role in the generation of disulfide bonds within G-CSF at the post-transcriptional level but not at the gene expression level. Thus, tumor ERO1-α plays a crucial role in the proper folding of G-CSF, leading to the augmented production of G-CSF. To further confirm our observations, we compared the gene

expression levels of *g-csf*, *cxcx1*, and *cxcl2* in SCR and KD cells. As expected, we did not observe any differences in mRNA levels of these genes between the two cell lines (Fig. 10C). In addition, we compared the redox states of G-CSF in SCR and KD cells. We found that the total amount of G-CSF protein in KD cells was much less than that in SCR cells under a reducing condition (Fig. 10D). Furthermore, both the reduced form and oxidized form of ERO1-α were clearly decreased in KD cells compared with those in SCR cells under a non-reducing condition . We speculated that the decrease in the total amount of G-CSF protein in KD tumor cells was due to degradation through ER-associated degradation because the immature reduced form of protein is destined to proteasomal degradation. This will be examined in the future. We concluded that tumor-associated ERO1-α facilitated the oxidative folding of factors including G-CSF, CXCL1m and CXCL2 for the induction and recruitment of PMN-MDSCs, resulting in the inhibition of antitumor T-cell response.

4. Discussion

Oxidative protein folding characterized by intramolecular disulfide bond formation

is the most common post-transcriptional modification[18]. A proper disulfide configuration provides the structural foundation for more nuanced intramolecular folding events that define protein activity[23]. Most of the proteins that are secreted or expressed on the cell surface have intramolecular disulfide bonds. Thus, oxidative protein folding is critical for normal cell function and homeostasis. Among the oxidoreductases expressed in the ER, ERO1-α is central to oxidative protein folding, but its expression varies in a tissue-specific manner[19]. Moreover, it has been shown that ERO1-α is upregulated under a hypoxic condition[24, 25], which is frequently observed in a cancer microenvironment. Furthermore, we previously showed that ERO1-α is overexpressed in various types of cancer cells line and cancer tissues[19]. Since cancer cells may take advantage of factors that are induced within hypoxic environments or at different stages of carcinogenesis, these finding led us to hypothesize that overexpression of ERO1-α might be functionally important for tumor cells, promoting further exploration of the role that ERO1-α might play in cancer progression. In this study, we found that suppression of ERO1-α protein resulted in a dramatic reduction of tumor growth using a mouse mammary gland cancer 4T1 model. Since the expression

of ERO1-α did not seem to play a major role in tumor cell growth *in vitro* or *in vivo* tumor growth using nude mice, massive infiltration of PMN-MDSCs was considered to contribute to tumor growth in BALB/c mice. In fact, an *in vivo* depletion assay using anti-Ly6G, anti-CD4 or anti-CD8 mAbs and a tumor rechallenge assay clearly showed that PMN-MDSCs inhibited anti-tumor T-cell responses. Since ERO1-α is a sulfhydryl oxidase[26], it is unlikely that ERO1-α would directly induce proliferation of PMN-MDSCs. Therefore, we measured levels of cytokines and chemokines responsible for the induction or recruitment of PMN-MDSCs in the culture supernatant. 4T1 tumor cells secreted a large amount of G-CSF. In contrast, ERO1-α knockdown cells showed decreased secretion of G-CSF, CXCL-1, and CXCL-2. Based on these results, we hypothesized that ERO1-α is involved in the proper oxidative protein folding of G-CSF before it is secreted and that the loss of ERO1-α leads to functionally inactive G-CSF (reduced form) as shown by Western blotting under a non-reducing condition (Fig. 10D). To further confirm that what we observed is a post-transcriptional event, we conducted real-time RT-PCR on SCR cells and KD cells. We did not observe any differences in mRNA levels of these genes between the two cell lines, suggesting that ERO1-α acted

at the post-translational level. Since ERO1-α-expressing 4T1 cells may affect the function of MDSCs through the production of some cytokines, this possibility should be investigated in the near future.

ERO1-α was previously reported by our group to be overexpressed in breast cancer tissues and to be useful as a poor prognostic marker[19]. Many tumors, including breast cancer, have the capacity to promote immune tolerance and escape host immune surveillance[2]. Tumors utilize numerous pathways to inhibit immune responses, including the elaboration of immune inhibitory cytokines such as IL-10 and TGF-β, as well as inducing host cells to release immune inhibitors. In addition to these mechanisms, immune suppression through MDSCs has a crucial role in promoting tumor progression[1].

In this study using a mouse mammary gland carcinoma 4T1 model, we showed that ERO1-α contributes to suppression of anti-tumor immunity through upregulation of G-CSF and CXCL1/2 via facilitation of oxidative protein folding. We did not determine whether ERO1-α is solely responsible for the proper oxidative folding of these molecules or whether it cooperates with protein disulfide isomerase (PDI) while these

molecules are folding in the ER and Golgi. These questions need to be clarified. While further research is still needed to understand the role of ERO1-α *in vivo*, the results presented here strongly suggest that targeted inhibition of ERO1-α may stall cancer progression.

References

[1] Gabrilovich DI, Nagaraj S. Myeloid-derived suppressor cells as regulators of the immune system. Nature reviews Immunology. 2009; 9: 162-74.

[2] Nagaraj S, Schrum AG, Cho HI, Celis E, Gabrilovich DI. Mechanism of T cell tolerance induced by myeloid-derived suppressor cells. Journal of immunology. 2010; 184: 3106-16.

[3] Khaled YS, Ammori BJ, Elkord E. Increased levels of granulocytic myeloid-derived suppressor cells in peripheral blood and tumour tissue of pancreatic cancer patients. Journal of immunology research. 2014; 2014: 879897.

[4] Meyer C, Sevko A, Ramacher M, et al. Chronic inflammation promotes myeloid-derived suppressor cell activation blocking antitumor immunity in transgenic mouse melanoma model. Proceedings of the National Academy of Sciences of the United States of America. 2011; 108: 17111-6.

[5] Song C, Yuan Y, Wang XM, et al. Passive transfer of tumour-derived MDSCs inhibits asthma-related airway inflammation. Scandinavian journal of immunology. 2014; 79: 98-104.

[6] Kujawski M, Kortylewski M, Lee H, Herrmann A, Kay H, Yu H. Stat3 mediates myeloid cell-dependent tumor angiogenesis in mice. The Journal of clinical investigation. 2008; 118: 3367-77.

[7] Oh K, Lee OY, Shon SY, et al. A mutual activation loop between breast cancer cells and myeloid-derived suppressor cells facilitates spontaneous metastasis through IL-6 trans-signaling in a murine model. Breast cancer research : BCR. 2013; 15: R79.

[8] Markowitz J, Wesolowski R, Papenfuss T, Brooks TR, Carson WE, 3rd. Myeloid-derived suppressor cells in breast cancer. Breast cancer research and treatment. 2013; 140: 13-21.

[9] Asano Y, Yokoyama T, Shibata S, et al. Effect of the chimeric soluble granulocyte colony-stimulating factor receptor on the proliferation of leukemic blast cells from patients with acute myeloblastic leukemia. Cancer research. 1997; 57: 3395-7.

[10] Chakraborty A, Guha S. Granulocyte colony-stimulating factor/granulocyte colony-stimulating factor receptor biological axis promotes survival and growth of bladder cancer cells. Urology. 2007; 69: 1210-5.

[11] Joshita S, Nakazawa K, Sugiyama Y, et al. Granulocyte-colony stimulating factor-producing pancreatic adenosquamous carcinoma showing aggressive clinical course. Internal medicine. 2009; 48: 687-91.

[12] Savarese TM, Mitchell K, McQuain C, et al. Coexpression of granulocyte colony stimulating factor and its receptor in primary ovarian carcinomas. Cancer letters. 2001; 162: 105-15.

[13] Waight JD, Hu Q, Miller A, Liu S, Abrams SI. Tumor-derived G-CSF facilitates neoplastic growth through a granulocytic myeloid-derived suppressor cell-dependent mechanism. PloS one. 2011; 6: e27690.

[14] Abrams SI, Waight JD. Identification of a G-CSF-Granulocytic MDSC axis that promotes tumor progression. Oncoimmunology. 2012; 1: 550-1.

[15] Frand AR, Kaiser CA. Ero1p oxidizes protein disulfide isomerase in a pathway for disulfide bond formation in the endoplasmic reticulum. Mol Cell. 1999; 4: 469-77.

[16] Appenzeller-Herzog C, Riemer J, Christensen B, Sorensen ES, Ellgaard L. A novel disulphide switch mechanism in Ero1alpha balances ER oxidation in human cells. EMBO J. 2008; 27: 2977-87.

[17] Appenzeller-Herzog C, Riemer J, Zito E, et al. Disulphide production by Ero1alpha-PDI relay is rapid and effectively regulated. EMBO J. 2010; 29: 3318-29.

[18] Araki K, Nagata K. Functional in vitro analysis of the ERO1 protein and protein-disulfide isomerase pathway. J Biol Chem. 2011; 286: 32705-12.

[19] Kutomi G, Tamura Y, Tanaka T, et al. Human endoplasmic reticulum oxidoreductin 1-alpha is a novel predictor for poor prognosis of breast cancer. Cancer science. 2013; 104: 1091-6.

[20] Acharyya S, Oskarsson T, Vanharanta S, et al. A CXCL1 paracrine network links cancer chemoresistance and metastasis. Cell. 2012; 150: 165-78.

[21] Katoh H, Wang D, Daikoku T, Sun H, Dey SK, Dubois RN. CXCR2-expressing myeloid-derived suppressor cells are essential to promote colitis-associated tumorigenesis. Cancer cell. 2013; 24: 631-44.

[22] Mo J, Tymiak AA, Chen G. Characterization of disulfide linkages in recombinant human granulocyte-colony stimulating factor. Rapid communications in mass spectrometry : RCM. 2013; 27: 940-6.

[23] Cabibbo A, Pagani M, Fabbri M, et al. ERO1-L, a human protein that favors disulfide bond formation in the endoplasmic reticulum. J Biol Chem. 2000; 275: 4827-33.

[24] Gess B, Hofbauer KH, Wenger RH, Lohaus C, Meyer HE, Kurtz A. The cellular oxygen tension regulates expression of the endoplasmic oxidoreductase ERO1-Lalpha. Eur J Biochem. 2003; 270: 2228-35.

[25] May D, Itin A, Gal O, Kalinski H, Feinstein E, Keshet E. Ero1-L alpha plays a key role in a HIF-1-mediated pathway to improve disulfide bond formation and VEGF secretion under hypoxia: implication for cancer. Oncogene. 2005; 24: 1011-20.

[26] Araki K, Inaba K. Structure, mechanism, and evolution of Ero1 family enzymes. Antioxid Redox Signal. 2012; 16: 790-9.

Figure legends

Figure 1.

Expression of ERO1-α within human breast cancer cell lines was enhanced compared with that in normal breast tissue. (A) Human ERO1-α mRNA levels in breast cancer cell lines (Luminal type: MCF7, BT-474, UACC-893; HER2 type: SK-BR-3; Triple negative breast cancer: MDA-MB-157, MDA-MB-231, MDA-MB-468) and normal breast tissue determined by real-time PCR. Data represent means ±SEM. * $P<0.05$, unpaired Student's t-test. Data are representative of three independent experiments. (B) Normal breast tissue and (C) breast cancer tissue were stained for ERO1-α (× 100, inset:× 200). Representative micrographs were shown.

Figure 2.

Knockdown of ERO1-α within 4T1 cells promoted cellular immunity against 4T1 cells. (A) Western blot analysis of 4T1 (WT) cells, scrambled shRNA-transfected (SCR) and ERO1-α knockdown (KD) cells. (B) Tumor growth rates of SCR and KD cells were compared using BALB/c nu/nu mice (five mice/group). Data represent means ±SEM.

(C) Tumor growth rates of SCR and KD cells were compared using BALB/c mice (eleven mice/group). Data represent means ±SEM. (D) Overall survival rates of SCR and KD cells were analyzed using BALB/c mice (twelve mice/group, scarified when tumor volume was over 800 mm^3). Data represent means ±SEM. * $p < 0.01$, unpaired Student's t-test. The experiment was repeated three times with essentially the same results.

Figure 3. Expression of ERO1-α within the tumor suppressed both CD4- and CD8-dependent cellular immunity.

(A) Mice were challenged with 3×10^4 4T1 SCR cells (five mice) or KD cells (twenty mice) into the left 4th mammary glands. For the depletion of CD4 and/or CD8 T cells, mice were divided into four groups (five mice/group) injected intraperitoneally with a rat IgG as a control, a CD4-specific antibody and/or CD8-specific antibody at 200 μg/mouse on day 3 before and day 1 after tumor challenge. Data represent means ±SEM. $^{\#}$ $p < 0.01$, Dunnet's test. (B) Mice that ERO1-α knockdown cells were re-challenged with 3×10^4 4T1 cells into the left 4th mammary glands (five mice). As a control,

BALB/c mice cells were challenged with 3 x 10^4 4T1 cells into the left 4th mammary glands (five mice). Tumor length and width were measured with a caliper. Data represent means ±SEM. $^{\dagger}p < 0.001$, Mann-Whitney' test. The experiment was repeated three times with essentially the same results.

Figure 4.

Enhanced expression of ERO1-α within 4T1 cells suppressed cellular immunity against 4T1 cells. (A) Western blot analysis of mock cells and ERO1-α-overexpressed (OE) cells. (B) Tumor growth rates of mock and OE cells were compared using BALB/c nu/nu mice (five mice/group). Data represent means ±SEM. (C) Tumor growth rates of mock and OE cells were compared using BALB/c mice (eight mice/group). Data represent means ±SEM. (D) Overall survival rates of mock and OE cells were analyzed using BALB/c mice (thirteen mice/group, scarified when tumor volume was over 800 mm^3). * $p < 0.05$, unpaired Student's t-test. The experiment was repeated three times with essentially the same results.

Figure 5.

Expression of ERO1-α significantly promoted peritumoral and intratumoral infiltration of $CD11b^+$ and $Gr\text{-}1^+$ granulocytic cells. The amount of peritumoral infiltration of inflammatory cells in SCR (A) was larger than that in KD (B) (x 40, inset: x 100). Immunohistochemical staining for CD11b (C, D) and Gr-1 (E, F) in SCR (C, E) and KD (D, F) tumor tissues (x 40, inset: x 100). (G) $CD11b^+$ cells in peritumoral and intratumoral sites were counted in five fields at x 200 magnification. Data represent means ±SEM. (H) $Gr\text{-}1^+$ cells in peritumoral and intratumoral sites were counted in five fields x 200 magnification. Data represent means ±SEM. * $p < 0.001$, Mann-Whitney test. Data are representative of three independent experiments.

Figure 6.

Knockdown of ERO1-α within 4T1 cells decreased infiltration of PMN-MDSCs in the body and peritumoral infiltration of PMN-MDSCs. (A) Splenocytes, (B) bone marrow, (C) peripheral blood leukocytes and (D) tumor-infiltrating leukocytes that expressed CD11b were divided into $CD11b^+$ $Ly6G^{hi}$ and $Ly6C^{int}$ cells by flowcytometric analysis.

3×10^4 events in splenocytes, bone marrow and peripheral blood leukocytes were analyzed, and 2.5×10^4 events in tumor-infiltrating leukocytes were analyzed. Data are representative of three independent experiments.

Figure 7.

Enhanced expression of ERO1-α within 4T1 cells increased the amount of PMN-MDSCs in the body and peritumoral infiltration of PMN-MDSCs. (A) Splenocytes, (B) bone marrow, (C) peripheral blood leukocytes and (D) tumor-infiltraing leukocytes that expressed CD11b were classified into $CD11b^+$ $Ly6G^{hi}$ and $Ly6C^{int}$ cells by flowcytometric analysis. 2.5×10^4 events in splenocytes, bone marrow, peripheral blood leukocytes and tumor-infiltrating leukocytes were analyzed. Data are representative of three independent experiments.

Figure 8.

Expression of ERO1-α within 4T1 cells promoted tumor growth by increasing the number of PMN-MDSCs in the body. Tumor growth rates of three groups were

compared using BALB/c mice (five mice/group). Mice were injected intraperitoneally with an Ly6G-specific antibody or Rat IgG at 100 μg/mouse every 2 days from day 15 (indicated by ↓) after tumor challenge. Data represent means ±SEM. * $p < 0.001$, Mann-Whitney test. The experiment was repeated three times with essentially the same results.

Figure 9.

Expression of ERO1-α within the tumor was involved in the production of G-CSF, CXCL1 and CXCL2. (A) Concentration of G-CSF in the 48-h culture supernatant from SCR or KD cells was measured using ELISA. (B) Concentrations of CXCL1 in the 24-h culture supernatant from SCR or KD cells was measured using ELISA. (C) Concentrations of CXCL2 in the 48-h culture supernatant from SCR or KD cells was measured using ELISA. (D) Concentration of G-CSF in the 48-h culture supernatant from mock or OE cells was measured using ELISA. (E) Concentrations of CXCL1 in the 24-h culture supernatant from mock or OE cells was measured using ELISA. (F) Concentrations of CXCL2 in the 48-h culture supernatant from mock or OE cells was

measured using ELISA. Data represent means ±SEM. * $p < 0.01$, unpaired Student's t-test. Data are representative of three independent experiments.

Figure 10.

Expression of ERO1-α within the tumor facilitated the production of CXCL1, CXCL2 and G-CSF via oxidative folding. (A) Cxcl1, cxcl2 and g-csf mRNA levels in mock and OE cells determined by qPCR analysis. Data represent means ±SEM. (B) Redox status of G-CSF in mock and OE cells was examined by Western blotting under reducing (R) or non-reducing (NR) conditions. Reduced form (R) or oxidized form (O) of G-CSF is indicated. (C) Cxcl1, cxcl2 and g-csf mRNA levels in SCR and KD cells determined by qPCR analysis. Data represent means ±SEM. (D) Redox status of G-CSF in mock and OE cells was examined by Western blotting under reducing (R) or non-reducing (NR) conditions. Reduced form (R) or oxidized form (O) of G-CSF is indicated. Data are representative of three independent experiments.

Figure 1

A

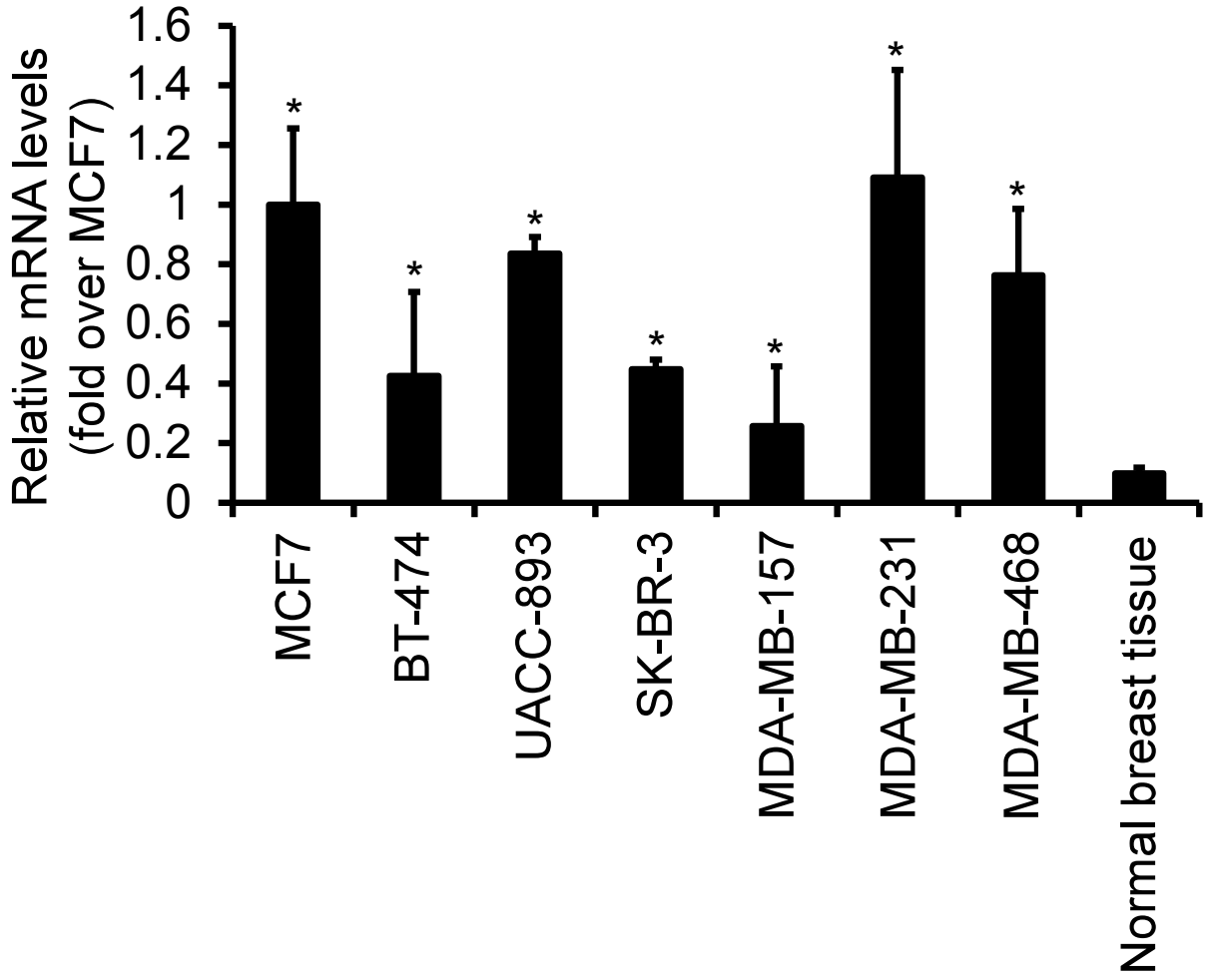
Relative mRNA levels
(fold over MCF7)
1.6
1.4
1.2
1
0.8
0.6
0.4
0.2
0
*
MCF7
BT-474
UACC-893
SK-BR-3
MDA-MB-157
MDA-MB-231
MDA-MB-468
Normal breast tissue

B

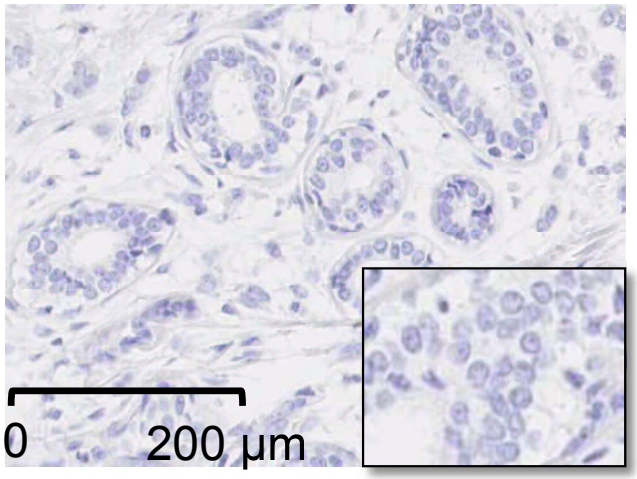
0
200 µm

C

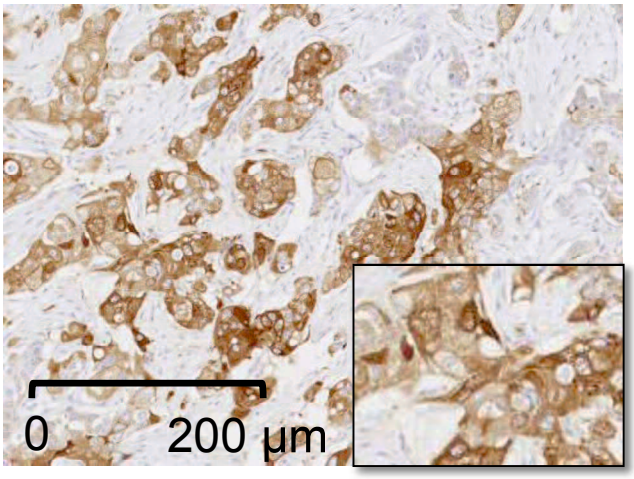
0
200 µm

Figure 2

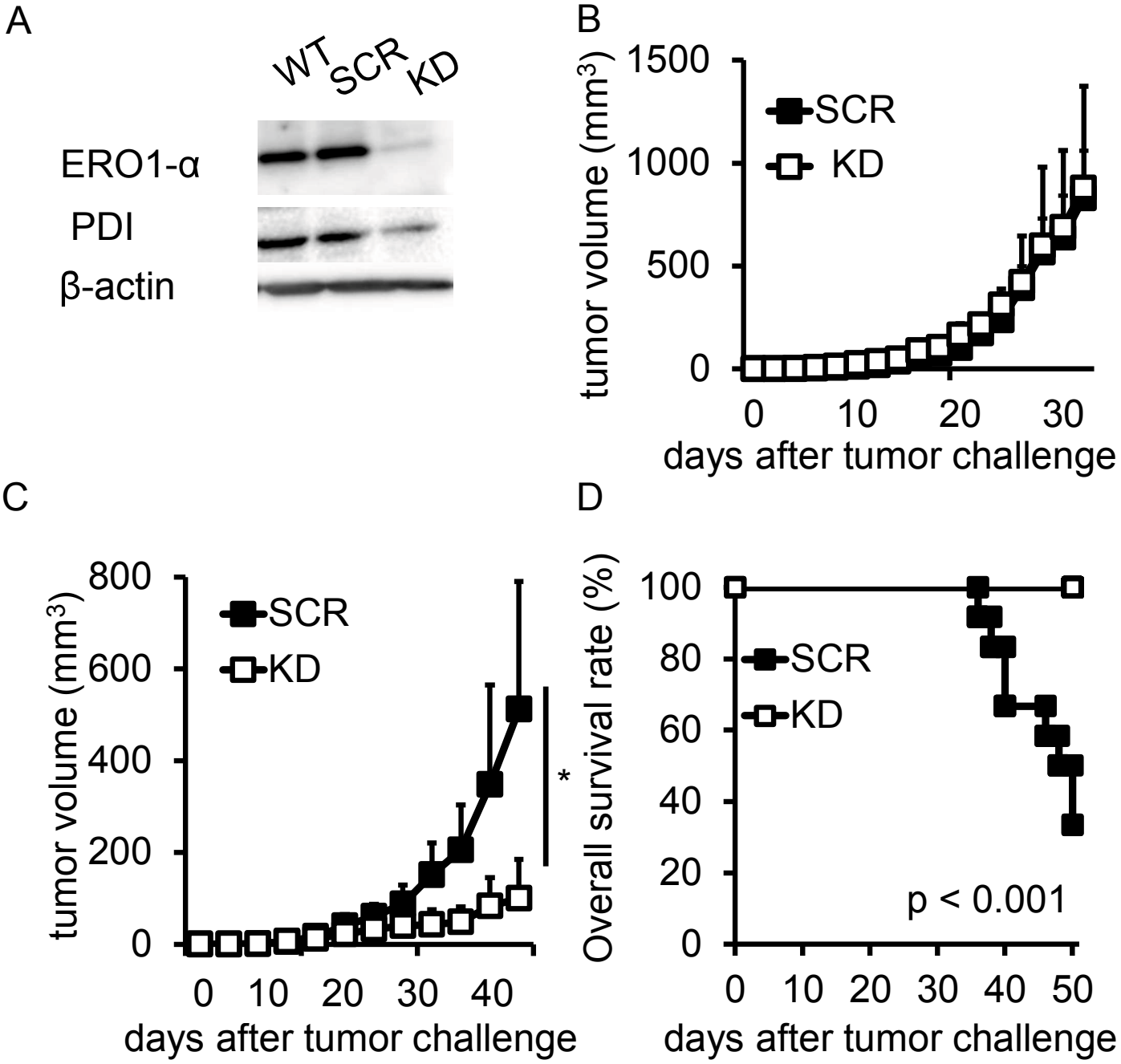
A
WT
SCR
KD
ERO1-α
PDI
β-actin
B
tumor volume (mm3)
1500
1000
500
0
SCR
KD
0
10
20
30
days after tumor challenge
C
tumor volume (mm3)
800
600
400
200
0
SCR
KD
*
0
10
20
30
40
days after tumor challenge
D
Overall survival rate (%)
100
80
60
40
20
0
SCR
KD
p < 0.001
0
10
20
30
40
50
days after tumor challenge

Figure 3

A

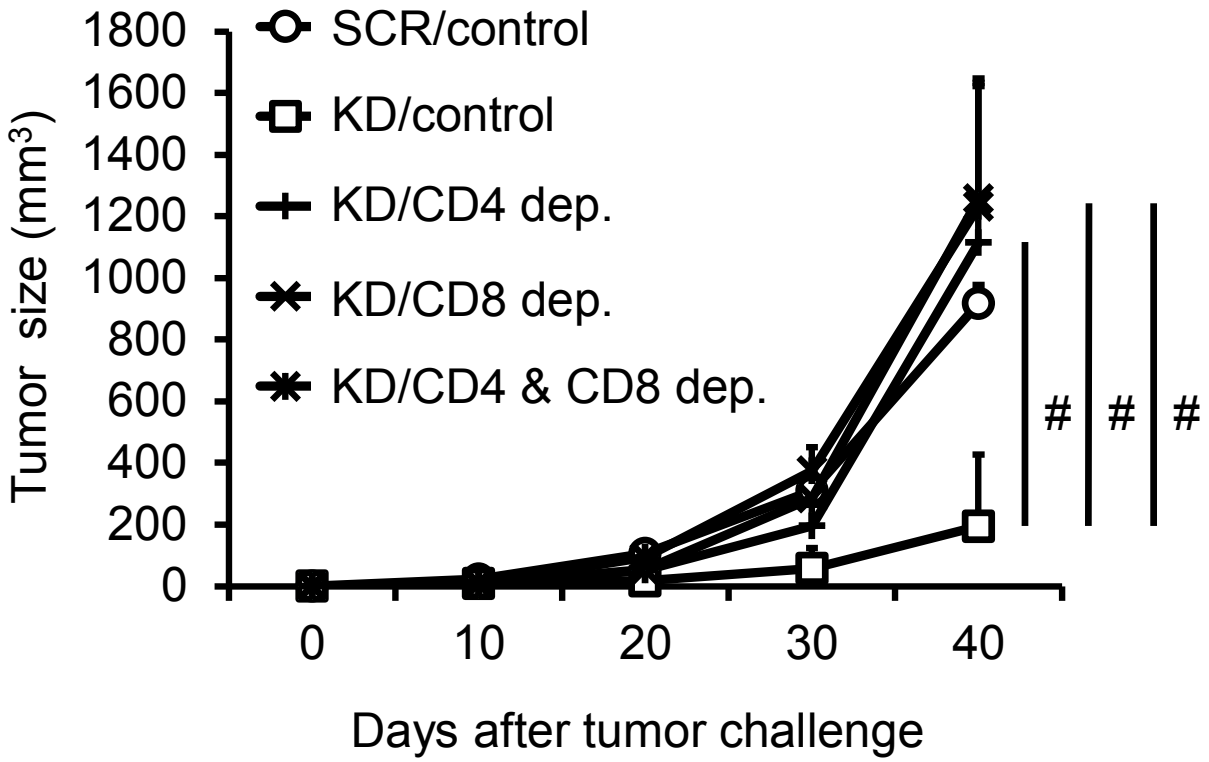
SCR/control
KD/control
KD/CD4 dep.
KD/CD8 dep.
KD/CD4 & CD8 dep.
Tumor size (mm3)
1800
1600
1400
1200
1000
800
600
400
200
0
0
10
20
30
40
Days after tumor challenge
#
#
#

B

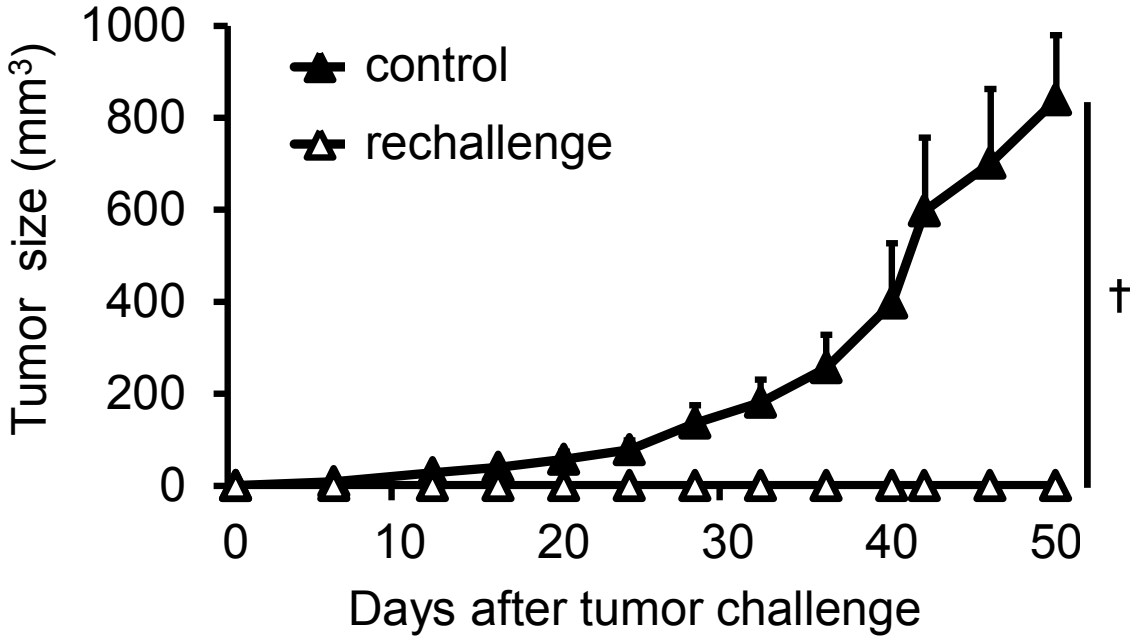
control
rechallenge
Tumor size (mm3)
1000
800
600
400
200
0
0
10
20
30
40
50
Days after tumor challenge
†

Figure 4

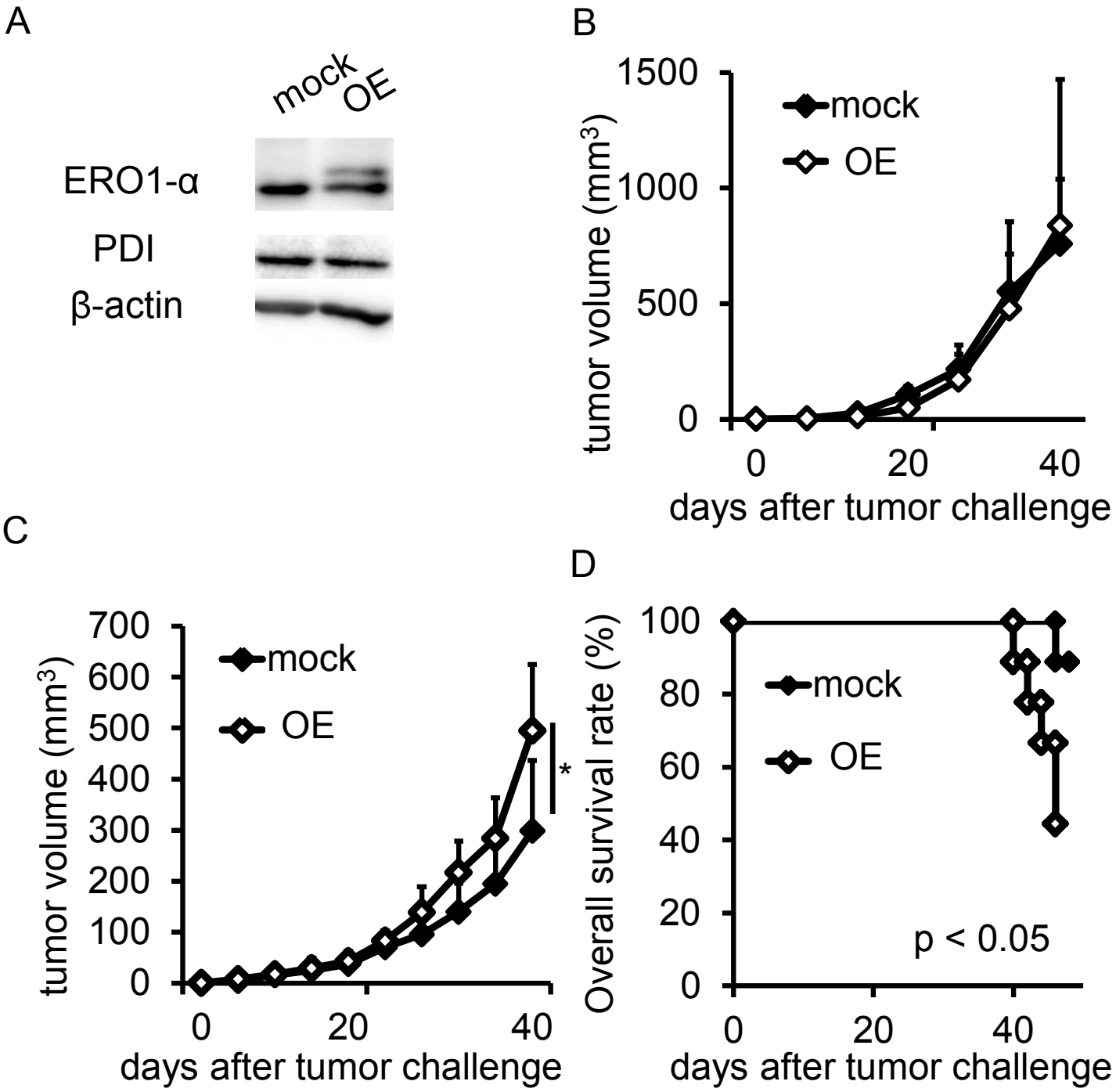
A
mock
OE
ERO1-α
PDI
β-actin
B
1500
1000
500
0
mock
OE
tumor volume (mm3)
0
20
40
days after tumor challenge
C
700
600
500
400
300
200
100
0
mock
OE
tumor volume (mm3)
*
0
20
40
days after tumor challenge
D
100
80
60
40
20
0
mock
OE
Overall survival rate (%)
p < 0.05
0
20
40
days after tumor challenge

Figure 5

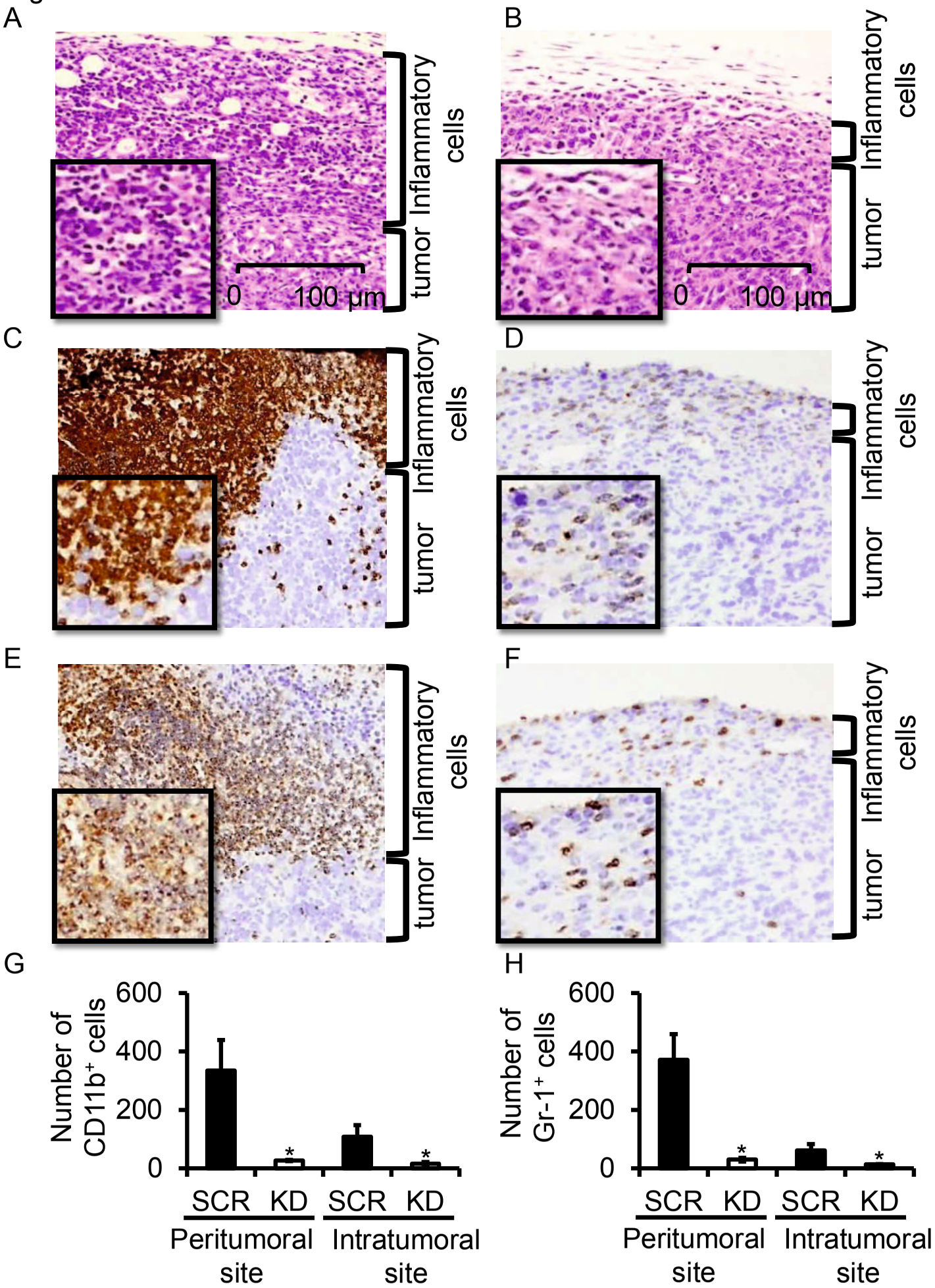
A
B
C
D
E
F
G
H
Inflammatory cells
tumor
0
100 μm
Number of CD11b+ cells
Number of Gr-1+ cells
600
400
200
0
SCR
KD
Peritumoral site
Intratumoral site

Figure 6

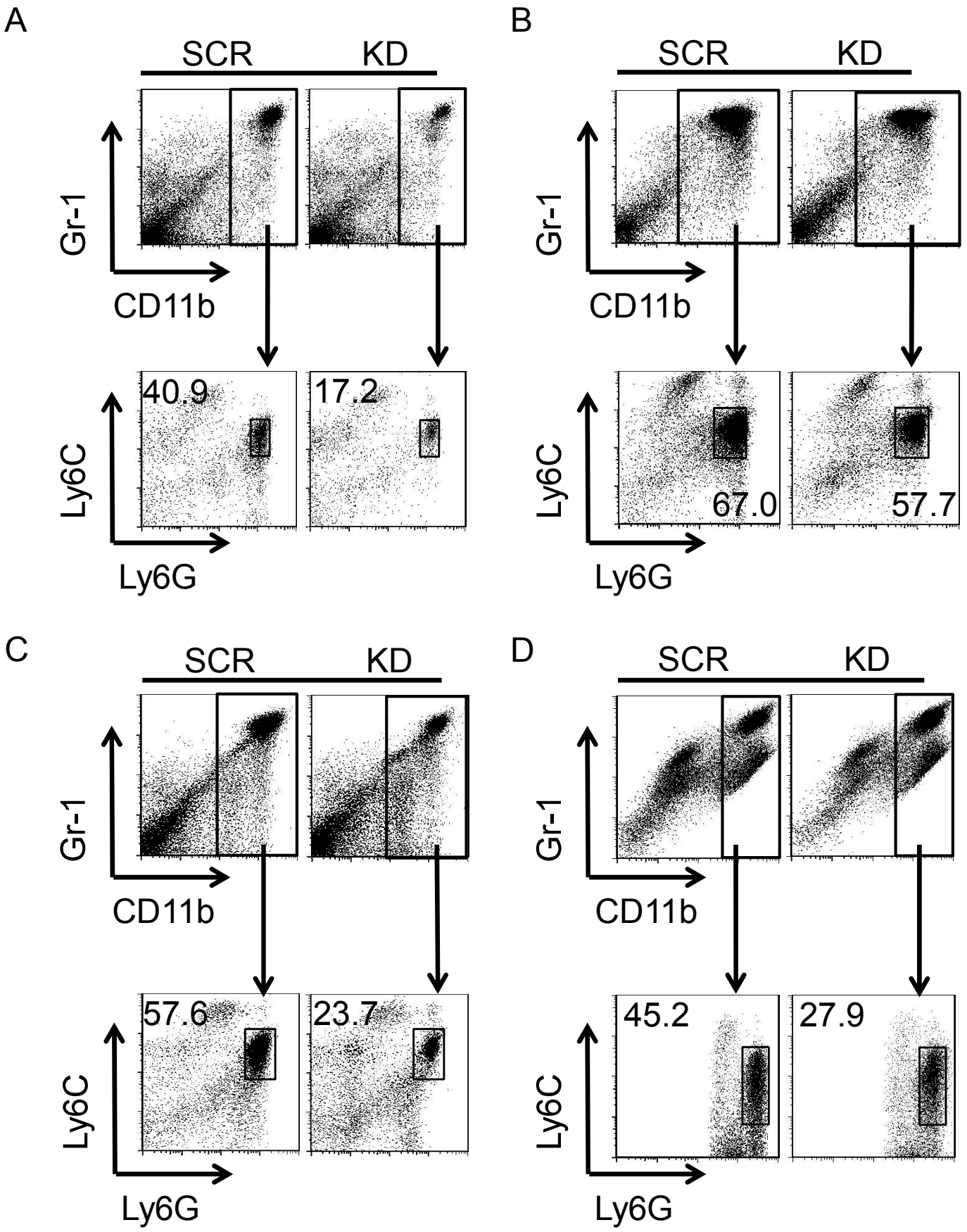
A
SCR
KD
Gr-1
CD11b
Ly6C
Ly6G
40.9
17.2
B
SCR
KD
Gr-1
CD11b
Ly6C
Ly6G
67.0
57.7
C
SCR
KD
Gr-1
CD11b
Ly6C
Ly6G
57.6
23.7
D
SCR
KD
Gr-1
CD11b
Ly6C
Ly6G
45.2
27.9

Figure 7

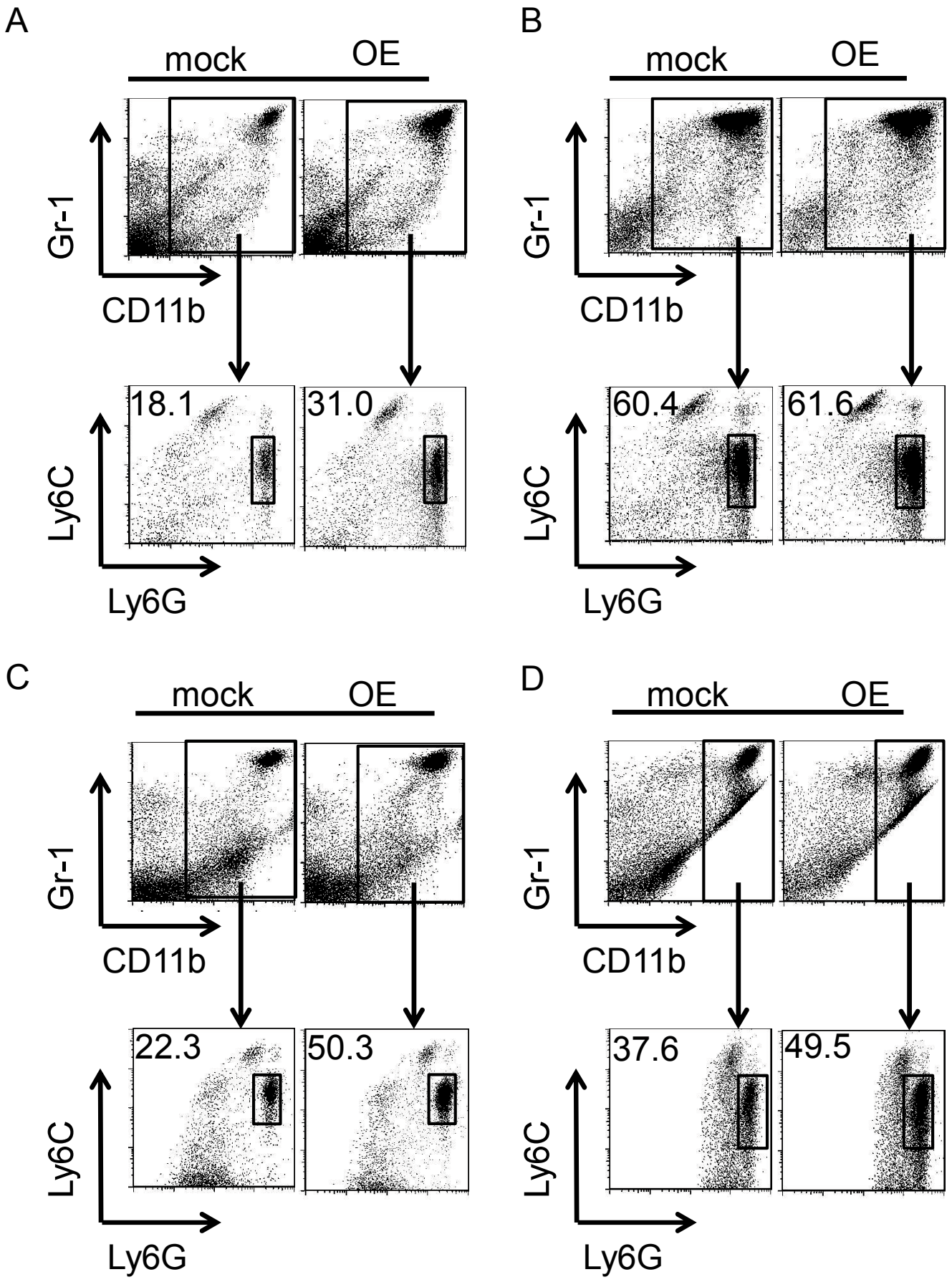
A
mock
OE
Gr-1
CD11b
18.1
31.0
Ly6C
Ly6G
B
mock
OE
Gr-1
CD11b
60.4
61.6
Ly6C
Ly6G
C
mock
OE
Gr-1
CD11b
22.3
50.3
Ly6C
Ly6G
D
mock
OE
Gr-1
CD11b
37.6
49.5
Ly6C
Ly6G

Figure 8

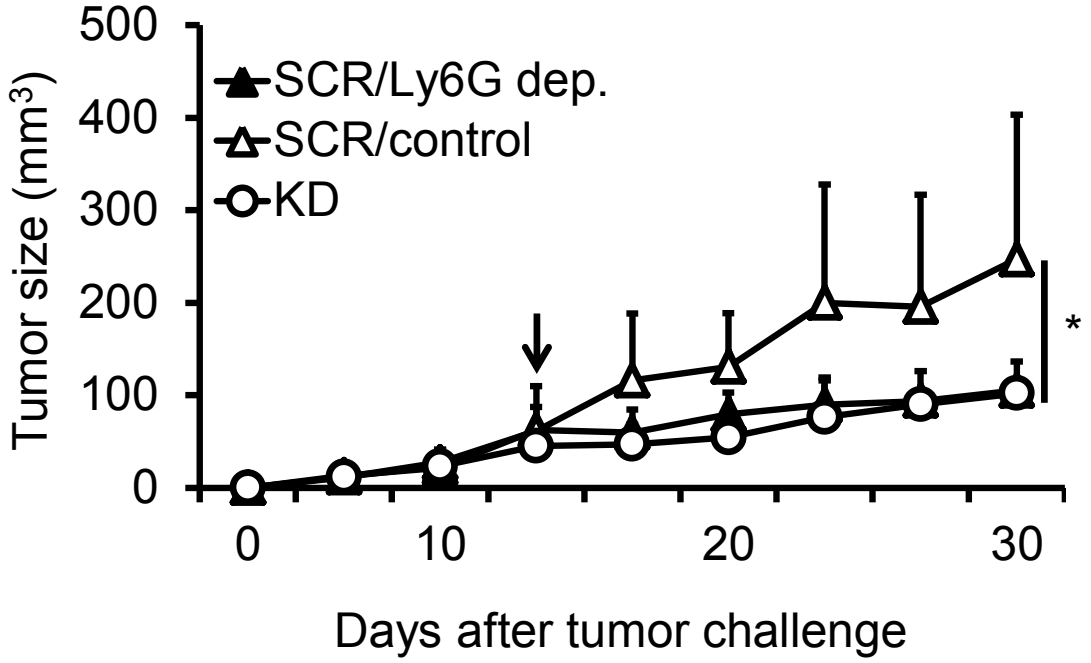
500
400
300
200
100
0
Tumor size (mm3)
SCR/Ly6G dep.
SCR/control
KD
*
0
10
20
30
Days after tumor challenge

Figure 9

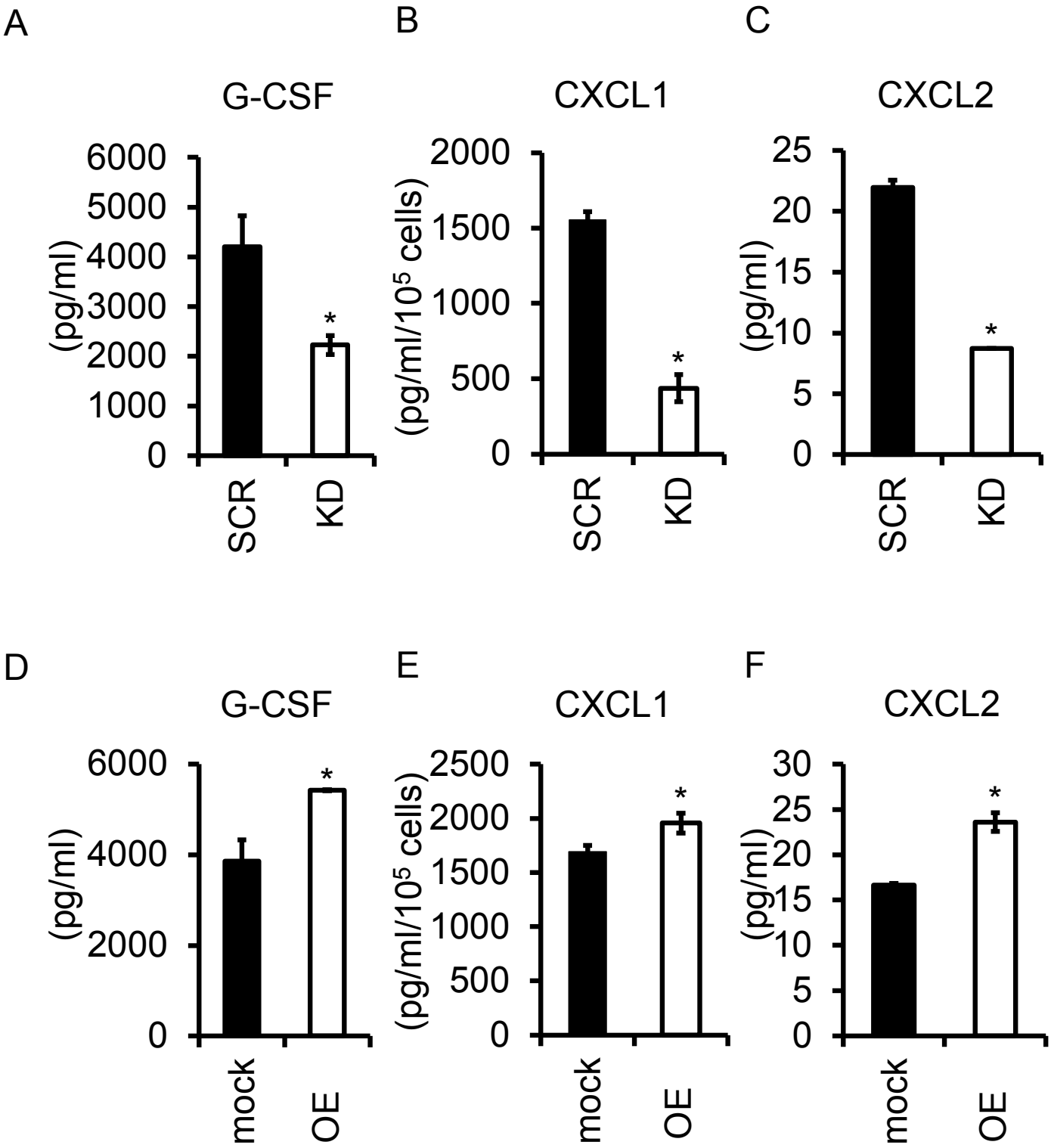
A
G-CSF
(pg/ml)
6000
5000
4000
3000
2000
1000
0
*
SCR
KD
B
CXCL1
(pg/ml/10^5 cells)
2000
1500
1000
500
0
*
SCR
KD
C
CXCL2
(pg/ml)
25
20
15
10
5
0
*
SCR
KD
D
G-CSF
(pg/ml)
6000
4000
2000
0
*
mock
OE
E
CXCL1
(pg/ml/10^5 cells)
2500
2000
1500
1000
500
0
*
mock
OE
F
CXCL2
(pg/ml)
30
25
20
15
10
5
0
*
mock
OE

Figure 10

A

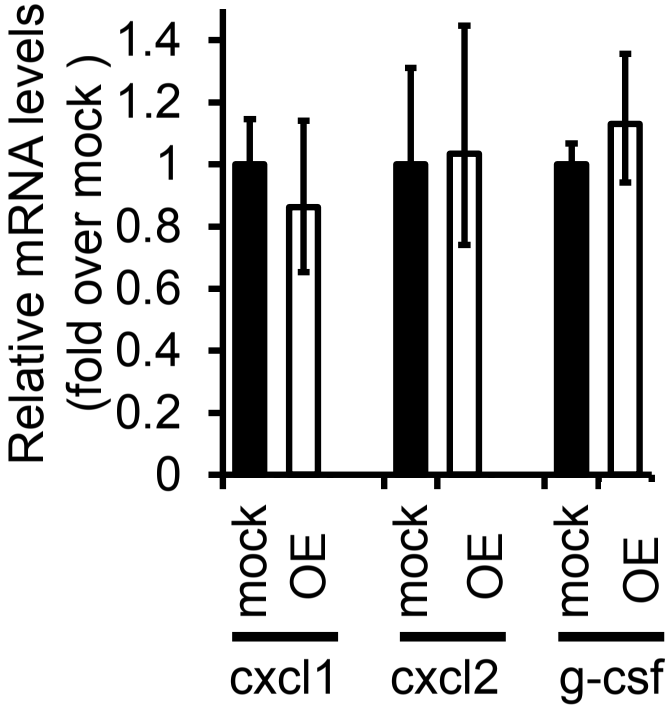

B

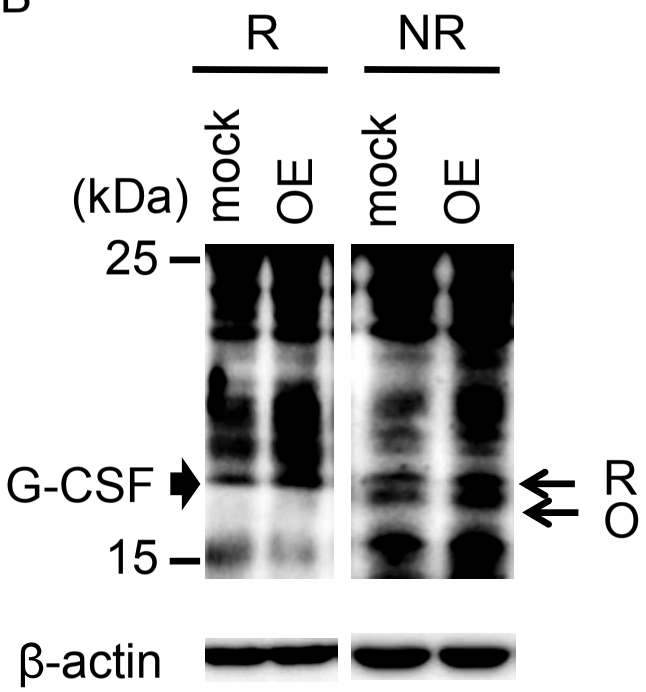

C

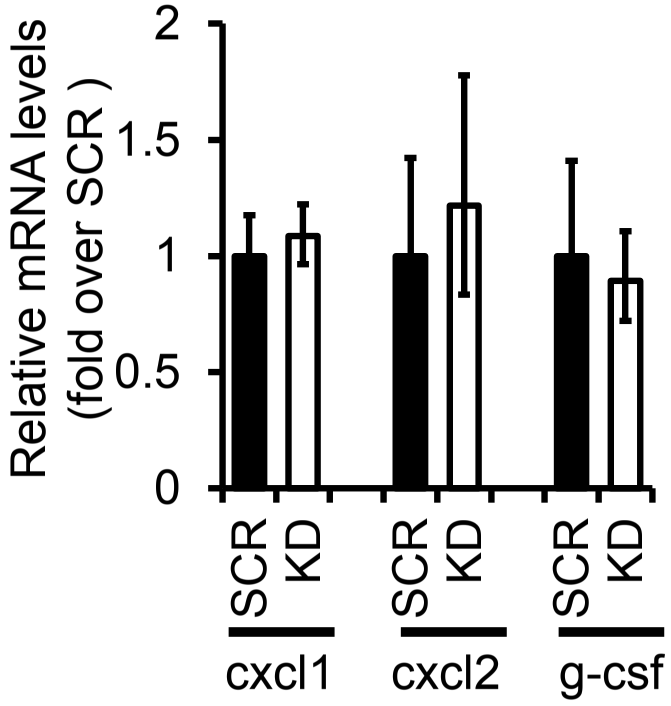

D

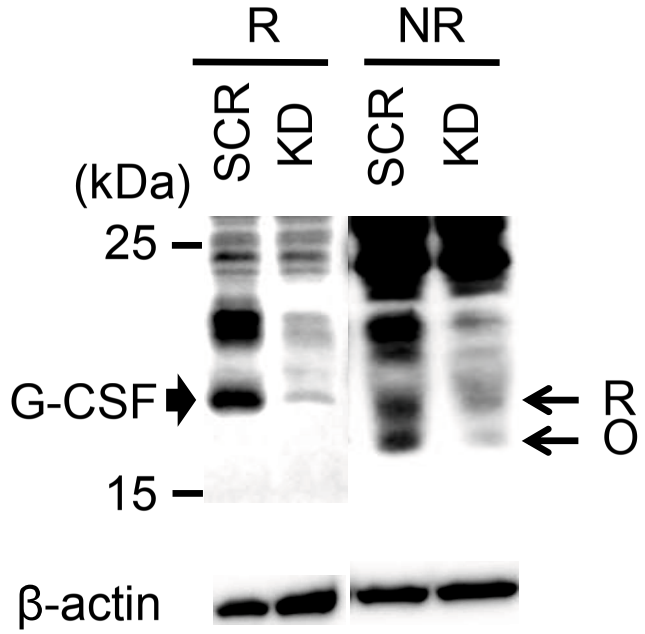

Supplemental materials and methods

In vitro tumor growth

5×10^4 SCR and KD cells were seeded at 5 x10^4 per well in a 10 cm dish. After 24, 48 and 72 h, cells were counted by using a Countess Automated Cell Counter (Life Technology, Carlsbad, CA, USA).

Flow cytometry

Peripheral blood, spleen cells and bone marrow were collected from BALB/c mice bearing SCR cells on day 28 after tumor challenge. Labeled 4T1 cells, peripheral blood, spleen cells and bone marrow were analyzed by a FACSCalibur flow cytometer (BD) and FlowJo (Tree Star Inc.). Antibodies reactive against the following cell surface markers were used (including appropriate isotype controls): PE-labeled CD11b (BioLegend), PerCP/Cy5.5-labeled Gr-1 (eBioscience) and APC-labeled CXCR2 (R&D Systems) .

Enzyme-linked immunosorbent assay (ELISA).

4T1 cells were plated at 1×10^5 cells／well in 6-well plates for 24 h. All samples were stored at −80°C until assayed. Mouse GM-CSF (R&D Systems, Minneapolis, MN, USA) levels were measured using a sandwich ELISA kit. Absorbance was determined at 450 nm.

Statistical analysis

Student's t-test was used for analysis of two unpaired samples. All analyses were carried out with STATMATE version 3.19 (ATMS Co., Ltd., Tokyo, Japan). A p-value of less than 0.05 was regarded as statistically significant. All statistical tests were two-sided.

Supplemental figure 1. Expression of ERO1-α within the tumor did not influence tumor growth *in vitro.*

SCR and KD cells were seeded at 5×10^4 per well in a 10 cm dish. After 24, 48 and 72 h, cells were counted by using a Countess Automated Cell Counter (Life Technology, Carlsbad, CA, USA). Data are representative of three independent experiments.

There were no differences of *in vitro* tumor growth of SCR cells and KD cells on days 1-3.

Supplemental figure 2. Effect of depletion of $Ly6G^+$ cells in peripheral blood leukocytes.

Peripheral blood leukocytes were collected from mice injected with the Ly6G antibody or rat IgG at 100 mg/mouse every 2 days from day 15 after the tumor challenge. They were divided into $CD11b^+$ $Ly6G^{hi}$ and $Ly6C^{int}$ cells. The percentage of $CD11b^+$ $Ly6G^{hi}$ in mice injected with the Ly6G antibody were lower (52.3%) than that in mice injected with rat IgG (70.8%). Data are representative of three independent

experiments.

Supplemental figure 3. Tumor ERO1-α facilitates the production of GM-CSF.

4T1 cells of SCR or KD were plated at 1×10^5 cells／well in 6-well plates for 24 h. All samples were stored at −80°C until assayed. Mouse GM-CSF (R&D Systems, Minneapolis, MN, USA) levels were measured using a sandwich ELISA kit. Absorbance was determined at 450 nm. Data are representative of three independent experiments.

The production of GM-CSF from SCR cells was shown to be greater than that from KD cells. * $p < 0.01$, unpaired Student's t-test.

Supplemental figure 4. CD11b$^+$ and Gr-1^{hi} cells (PMN-MDSC) expressed CXCR2 on the cell surface.

Peripheral blood, spleen cells and bone marrow were collected from BALB/c mice bearing SCR cells on day 28 after tumor challenge. Flow cytometric analysis of CXCR2

expression on these cells (solid line). These cells incubated with APC-labeled isotype control served as background controls (dashed line). Data are representative of three independent experiments.

Supplemental Table. 1 Expression of ERO1-α within the tumor affected the number of PMN-MDSCs in mice bearing the tumor.

(A) The number of PMN-MDSCs in bone marrow, spleen, peripheral blood leukocytes and tumor-infiltrating leukocytes in SCR group was higher than that in KD group. (B) The total numbers of PMN-MDSCs in bone marrow, spleen, peripheral blood leukocytes and tumor-infiltrating leukocytes in OE group were higher than that in mock group. Cells were analyzed in three independent studies. Data represent mean ± SEM. * $p < 0.01$, ** $p < 0.001$, Mann-Whitney test.

Supplemental figure 1

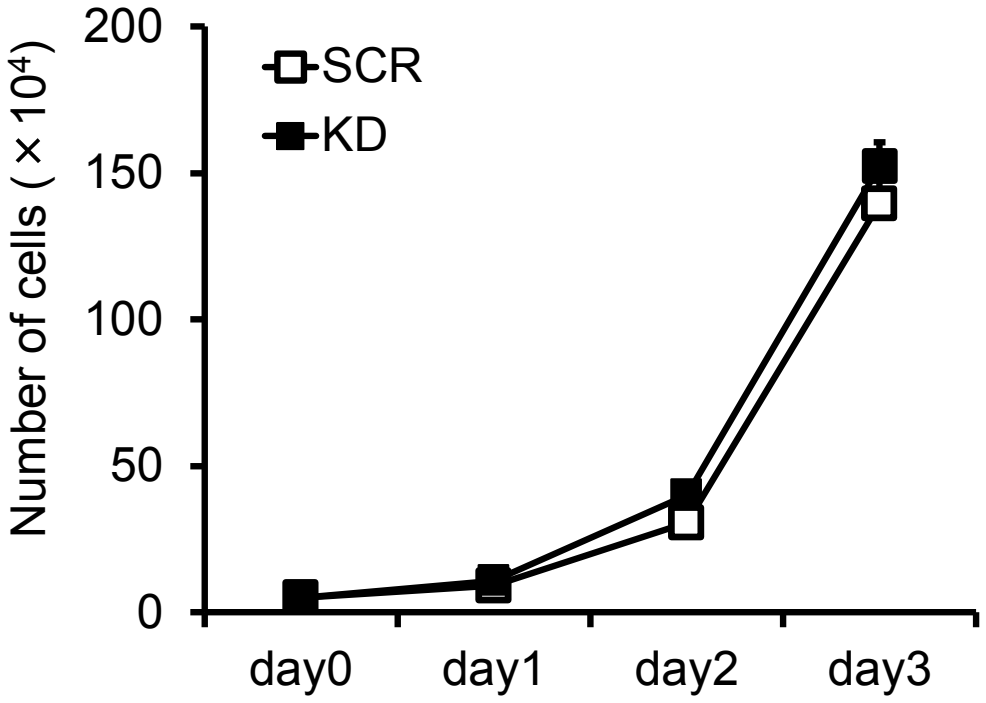

Supplemental figure 2

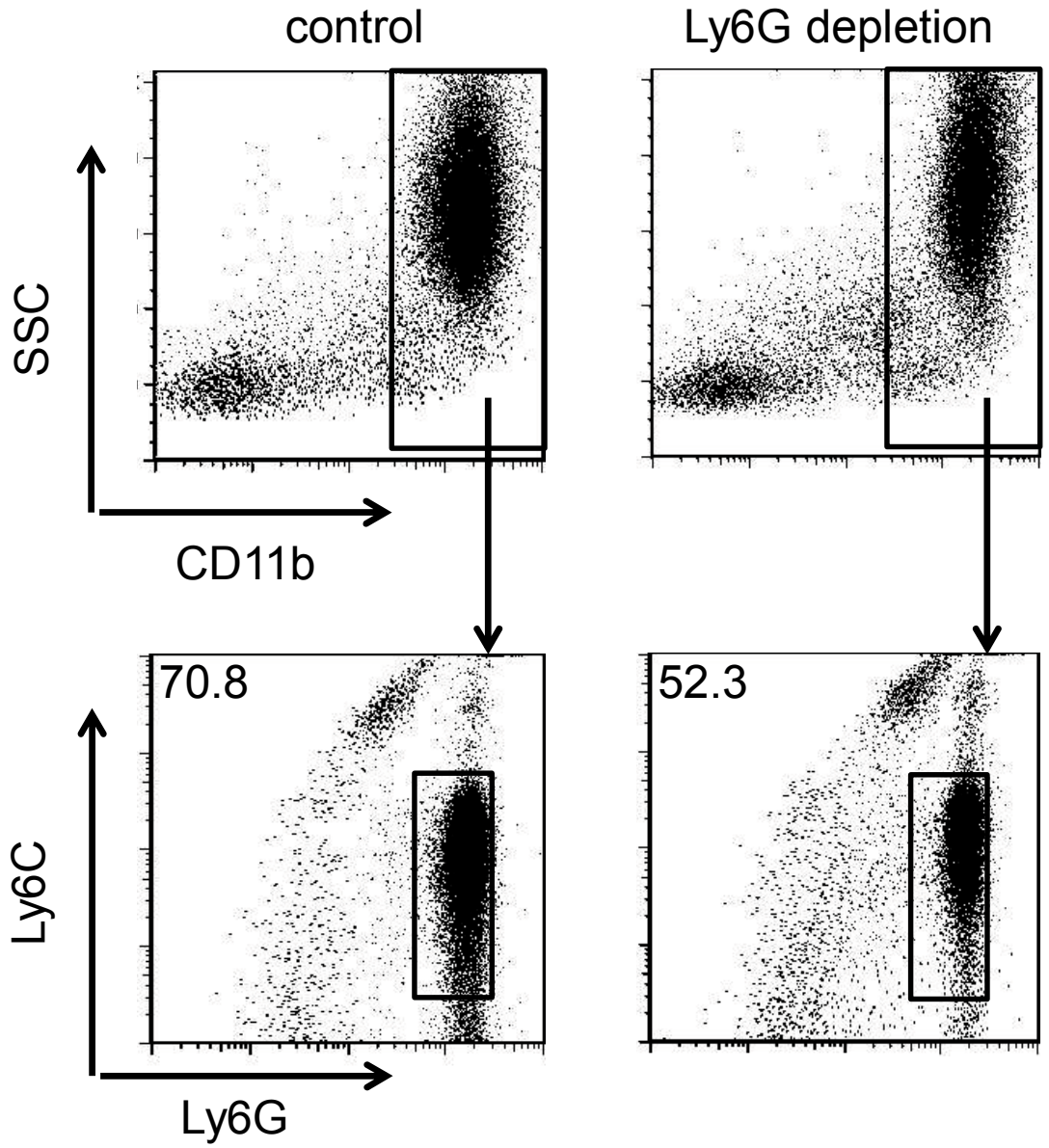

Supplemental figure 3

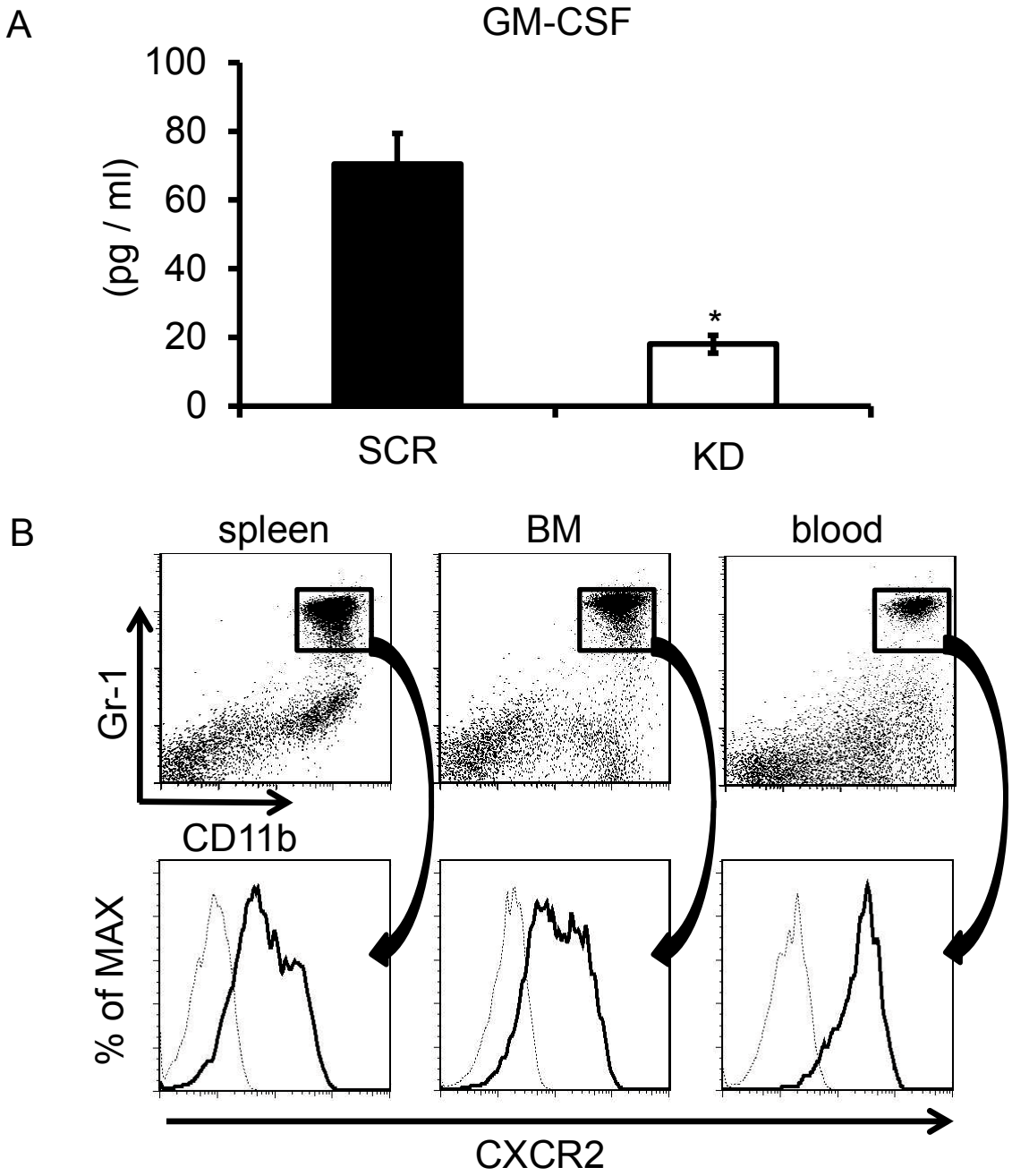

supplemental Table 1.

A

	SCR	KD
spleen	12104.7±971.6	5133.5±276.9**
bone marrow	19896.5±464.8	17242.5±108.4*
peripheral blood leukocytes	17529.6±143.0	7324.6±552.3**
tumor-infiltrating leukocytes	11344.9±578.9	7105.2±392.3*

(cells)

B

	mock	OE
spleen	4592.9±125.0	7604.4±262.8**
bone marrow	15279.6±260.4	15826.6±303.1**
peripheral blood leukocytes	5673.6±214.4	12125.4±721.1**
tumor-infiltrating leukocytes	9332.6±317.3	12492.4±484.3*

(cells)

Conclusion

The complex of peptide and Hsp90 can induce the larger amount of peptide-specific CD8 T cells than only peptide and only Hsp90 via promoting cross presentation.

The expression of ERO1-α in the tumor tissues inhibited immune response against tumors via stimulating the proliferation and recruitment of PMN-MDSCs.

Acknowledgments

I wish to pay sincere acknowledgement to Professor Yoshiharu Okamoto, Department of Veterinary Clinical Medicine, Joint School of Veterinary Medicine, Tottori University, for his sincere supervising and encouragement during the present investigation.

I also wish to thank Professor Yasuho Taura, Joint Faculty of Veterinary Medicine, Yamaguchi University; Professor Takashi Takeuchi, Department of Veterinary Clinical Medicine, Joint School of Veterinary Medicine, Tottori University; Professor Tomohiro Imagawa, Department of Veterinary Clinical Medicine, Joint School of Veterinary Medicine, Tottori University; Associated Professor Tomohiro Osaki, Department of Veterinary Clinical Medicine, Joint School of Veterinary Medicine, Tottori University, for their helpful suggestion as co-supervisor.

I am grateful to Professor Noriyuki Sato, Sapporo Medical University; Professor Koichi Hirata, Sapporo Medical University; Professor Yasuaki Tamura, Laboratory of Molecular Therapeutics, Center for Food and Medical Inovation, Hokkaido University; Associated Professor Toshihiko Torigoe, Sapporo Medical University; Lecture Yoshihiko Hirohashi, Sapporo Medical University; Lecture Tomohide Tsukahara,

Sapporo Medical University; Lecture Goro Kutomi, Sapporo Medical University; Assistant professor Takayuki Kanaseki, Sapporo Medical University; Dr. Koichi Okuya, Sapporo Medical University; Dr. Akari Takaya, Sapporo Medical University; Dr. Toshimitsu Kajiwara, Sapporo Medical University.

The study of Chapter I was supported in part by Health and labor Sciences Research Grant-in-Aid from Ministry of Health, Labor and Welfare of Japan. The study of Chapter II was supported in part by a Grant-in-Aid for Scientific Research from The Ministry of Education, Culture, Sports, Science and Technology of Japan.

Finally, I wish to express special thanks to my family, especially to my parents Masaru and Masumi for their hearty supports.